AD-A132 879 MOLECULAR SUEERSONIC JET STUDIES OF ANILINE SOLVATION BY HELIUM AND METHA..(U) COLORADO STATEUUNIV FORT COLLINS DEPT OF CHEMISTRY E R BERNSTEIN ET AL. 1/1

UNCLASSIFIED 16 SEP 83 TR-12 N00014-79-C-0647 F/G 7/3 NL

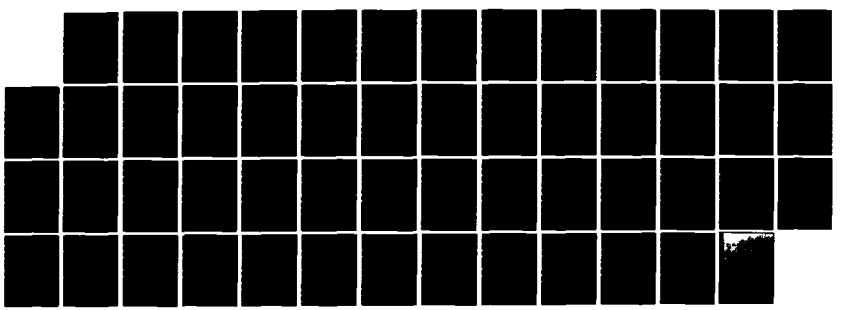

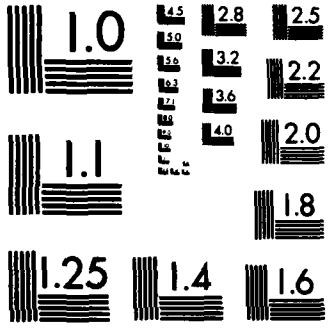

MICROCOPY RESOLUTION TEST CHART
NATIONAL BUREAU OF STANDARDS-1963-A

OFFICE OF NAVAL RESEARCH
Contract N00014-79-C-0647
TECHNICAL REPORT #12

MOLECULAR SUPERSONIC JET STUDIES OF ANILINE SOLVATION BY HELIUM AND METHANE

by

E.R. Bernstein, K. Law, and Mark Schauer

Prepared for Publication
in the
Journal of Chemical Physics

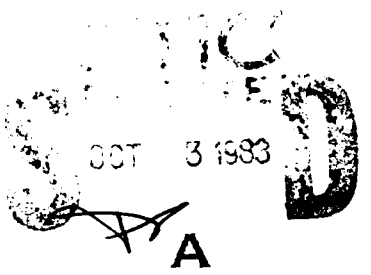

Department of Chemistry
Colorado State University
Fort Collins, Colorado 80523

September 16, 1983

REPORT DOCUMENTATION PAGE

READ INSTRUCTIONS BEFORE COMPLETING FORM

1. REPORT NUMBER: Technical Report #12	2. GOVT ACCESSION NO.
3. RECIPIENT'S CATALOG NUMBER	
4. TITLE (and Subtitle): Molecular Supersonic Jet Studies of Aniline Solvation by Helium and Methane	5. TYPE OF REPORT & PERIOD COVERED: Technical Report
6. PERFORMING ORG. REPORT NUMBER	
7. AUTHOR(s): E.R. Bernstein, K. Law, Mark Schauer	8. CONTRACT OR GRANT NUMBER(s): N00014-79-C-0647
9. PERFORMING ORGANIZATION NAME AND ADDRESS: Colorado State University, Department of Chemistry, Fort Collins, Colorado 80523	10. PROGRAM ELEMENT, PROJECT, TASK AREA & WORK UNIT NUMBERS
11. CONTROLLING OFFICE NAME AND ADDRESS: Office of Naval Research, Arlington, Virginia 22217	12. REPORT DATE: September 16, 1983
	13. NUMBER OF PAGES: 52
14. MONITORING AGENCY NAME & ADDRESS (if different from Controlling Office)	15. SECURITY CLASS. (of this report): Unclassified
	15a. DECLASSIFICATION/DOWNGRADING SCHEDULE

16. DISTRIBUTION STATEMENT (of this Report)

This document has been approved for public release and sale; its distribution is unlimited.

17. DISTRIBUTION STATEMENT (of the abstract entered in Block 20, if different from Report)

18. SUPPLEMENTARY NOTES

19. KEY WORDS (Continue on reverse side if necessary and identify by block number)

time of flight mass spectroscopy, two photon ionization, supersonic molecular jet, intramolecular vibrational distribution, van der Waals clusters, dispersed emission, fluorescence excitation.

20. ABSTRACT (Continue on reverse side if necessary and identify by block number)

The technique of two color resonant two photon ionization coupled with time of flight mass spectroscopy has been employed to study Aniline-He ($AnHe_x$) and Aniline-CH_4 ($An(CH_4)_x$) van der Waals clusters generated in a supersonic molecular jet. This technique allows identification of spectroscopic transitions with clusters of known mass because no ion fragmentation is observed. Specific features in the optical fluorescence excitation and dispersed emission spectra can thereby be uniquely identified with a

particular cluster. Cluster vibrations can be analyzed by a Morse potential to yield the An-He bond dissociation energy D_0 ~ 100 ± 50 cm^{-1}. Careful analysis of the dispersion emission from $AnHe_x$ suggests 145 < D_0 < 155 cm^{-1}. It is found that the van der Waals bond stretching frequency is nearly the same in the ground and excited states and that there is a strong propensity rule for $\Delta V = 0$ (V = vdW bond mode) as expected in this case, although $\Delta V = \pm 1$ transitions can be observed. The $AnHe_1$ and $AnHe_2$ origins are slightly red shifted with respect to the An origins, while the $AnHe_x$ ($x \geq 3$) origin is broad and nearly unshifted. This pattern is followed for $An(CH_4)_x$ clusters; $AnCH_4$ transitions are red shifted 80 cm^{-1} from the comparable An feature. The $An(CH_4)_x$ ($x \geq 3$) transitions appear at ~200-300 cm^{-1} below their comparable An mode. The binding energy for the An-CH_4 bond is found to be 500 < D_0 < 700 cm^{-1} in the $^1B_2$ state of aniline. Aniline has a strong preference for binding the solvent above and below the aromatic ring; it is argued that the third solvent species coordinates near the NH_2 moiety. Since the D_0 is large for An-CH_4 and the stretching mode is only ~25 cm^{-1} the $An(CH_4)_x$ system builds up a large density of states in the van der Waals degrees of freedom. This density of states allows intramolecular vibrational redistribution (IVR) to take place, if the An mode excited is lower in energy than the D_0 value. The rate of IVR from $6a^1_0$ (0^0_0 + 500 cm^{-1}) is somewhat faster than the 5 ns fluorescence rate but much slower than the rate of VP from higher levels. Both the IVR process, due to the van der Waals vibrational density of states, and the limiting solvent red shift, at a value similar to that found for cryogenic solutions, are discussed in terms of these clusters as model solute/solvent systems.

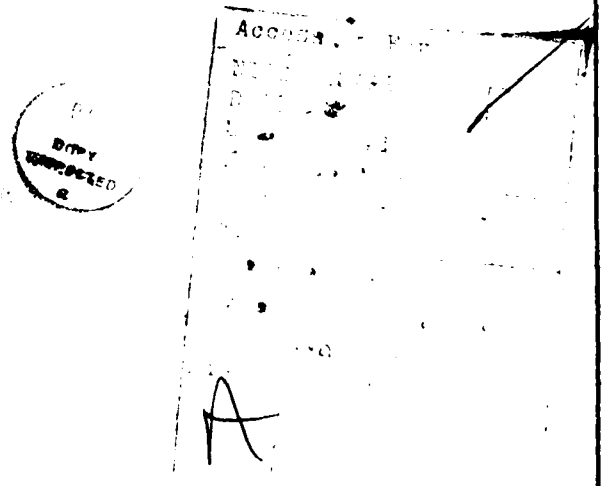

I. INTRODUCTION

It is well known that the supersonic molecular jet is a powerful tool for generating and studying weakly bound van der Waals (vdW) clusters.[1] Clusters formed between a large central molecule and one or more carrier gas species can be thought of as a microscopic solution. The solvation of the seeded molecule can be monitored spectroscopically as experimental parameters such as nozzle backing pressure (P_o), nozzle diameter and concentration of solvent species are varied.[2] However, often the stoichiometry of the cold cluster generated in the beam cannot be unambiguously determined by optical techniques. Monitoring the intensity of certain spectral features as P_o is changed can identify the particular feature as a cluster related transition[3], but these studies are not always definitive, especially in cases for which congestion in the spectral region is substantial.

Experiments using mass spectroscopy can give information about cluster size. However, electron impact or one-color multiphoton ionization techniques can impart excess energy to the cluster and cause fragmentation.[4] The technique of two color resonant two-photon ionization time of flight mass spectroscopy (2-color MS) can be used to ionize the clusters without fragmentation.[5] Using this technique, it is possible to obtain absorption spectra of an unambiguously mass-identified vdW cluster. Thus, the 2-color MS experiment greatly enhances the ability to interpret fluorescence excitation (FE) and dispersed emission (DE) spectra obtained from species generated in the beam.

In a previous publication, hereafter referred to as I,[6] we have addressed the relaxation mechanisms of aniline (An) and aniline-helium ($AnHe_x$) in the

jet, as well as various spectroscopic properties of the $AnHe_x$ clusters. The 2-color MS studies reported in the present paper contribute to a better understanding of $AnHe_x$ clusters with regard to relaxation processes and energy levels.

Several aspects of the An-CH_4 system have also been explored. These studies emphasize that 2-color MS experiments are essential to the study of vdW clusters and that they complement the FE and DE techniques. The 2-color MS experiment can be used to identify the origins and vdW vibrations associated with $(An(CH_4)$ and $An(CH_4)_2$ vibronic transitions. With this information it is possible to assign several cluster DE spectra. It is found that the vdW stretching frequency is nearly identical in the ground and excited states and that vibronic transitions evidence a strong $\Delta V = 0$ (in which V is some quantum of the vdW stretch) propensity rule. Also, it is demonstrated that attaching a CH_4 molecule to An increases the density of states in the system to the point at which the rate of intramolecular vibrational redistribution (IVR) becomes comparable to the rate of fluorescence. Therefore, the kinetics of energy flow in the excited state may be addressed.

The Results and Discussion sections of this paper are each divided into two parts. First, new information concerning the An-He system will be presented and discussed in terms of their significance for I. Second, the results of FE, DE, and 2-color MS studies of the An-CH_4 system will be shown and the similarities and differences between the An-He and An-CH_4 systems will be addressed.

II. EXPERIMENTAL PROCEDURES

The molecular jet apparatus and procedures for obtaining FE and DE spectra have been described in detail in I. Beam conditions are the same as described in I except for changes in P_o as indicated in the figure captions. The procedures for mixing gases and obtaining 1-color and 2-color MS spectra will be presented here.

To obtain a mixture of three components in the gas phase, a modification of the previous gas mixing system was necessary. The solvent gas (methane) is premixed with the carrier gas (helium) in an 1800 ml stainless steel cylinder. The concentration is determine by pressurizing a known volume (42 ml) of the system manifold, then opening the alloquate to the cylinder. The cylinder is then pressurized (to ca. 2000 psia) with carrier gas. Complete mixing is achieved by turbulence, greatly assisted by delivery through a long perforated fill tube within the cylinder, during the rapid pressurization process. This mixture is then regulated to the desired P_o and passed through a trap containing the solute (liquid aniline). The optimum concentration of solvent is determined by optimizing the absorption signal of the desired species observed through the particular detection technique being used (eg. FE, 2-color MS). The error in the quoted concentrations of solvent is less than 5%. The solute trap is not heated and the concentration of solute varies with P_o. Research grade methane and aniline, and commerical grade helium are used.

Both 1-color and 2-color resonance enhanced two photon ionization time of flight mass spectra were obtained for the An-He and An-CH_4 systems. 1-color MS involves 2-photon ionization of the species of interest. The ion production is greatly enhanced if the first photon is equal in energy to a vibronic

transition of the cluster. Therefore, if the intensity of the ion signal in a particular mass channel is monitored as the laser frequency is tuned, an absorption spectrum of the species corresponding to the mass channel being monitored is obtained.

Two color mass spectroscopy can provide information on van der Waals clusters which is not readily attainable through 1-color MS studies. For aniline, the absorption of the second photon in a 1-color MS experiment provides ~7000 cm^{-1} of excess vibration energy to a cluster ion which causes substantial fragmentation of the ion. 2-color MS experiments require two laser beams, the first excites the species of interest to its first excited state (ν_{pump}), and the second beam excites the species to create the ion (ν_{ion}). These two beams are supplied by two Nd:YAG pumped dye laser systems (Quanta Ray). The two lasers are synchronized by triggering one from the other and relative jitter in the light pulses in $\lesssim$5 ns as measured by a 1P28 phototube. The ionization thresholds of An, $AnHe_x$ and $An(CH_4)_x$ at various vibronic levels are determined by scanning ν_{ion} while keeping ν_{pump} constant. The pump beam intensity is reduced to the point at which no signal is observed without ν_{ion}. These procedures assure that very little fragmentation of the vdW clusters occurs.

Experimental conditions for obtaining the spectra are described in the figure captions. The peaks in the DE spectra are slit width limited at ~15 cm^{-1} unless otherwise stated. FE, 1-color and 2-color MS linewidths are only limited by the frequency width of the lasers, ~0.25 cm^{-1}. The spectra are calibrated using the opto-galvanic effect with an Fe-Ne hollow cathode lamp.[7]

III. RESULTS

A. An-He System

As pointed out in the last section, much less fragmentation of vdW species is observed in the 2-color than in the 1-color MS experiment. This is readily seen by comparing Fig. 1 and Fig. 2. In 1-color MS (Fig. 1) absorption features due to AnHe and $AnHe_2$ are present in the absorption spectrum taken while gating on the An mass channel. Also, absorption features due to $AnHe_2$ appear in the AnHe spectrum. While the 1-color MS are distorted by fragmentation, they are more intense than the corresponding 2-color spectra; it thus is possible to obtain 1-color mass spectra, but not 2 color mass spectra, of the $AnHe_3$ species as the $AnHe_3$ peaks are considerably broader and weaker than the smaller cluster peaks. Also, the shift of the $AnHe_3$ 0_0^0 relative to the An 0_0^0 is different than would be predicted based on the AnHe and $AnHe_2$ spectral shifts. It appears that the third He may attach to a different position on the An than the first two.

The 2-color mass spectra show clearly the undistorted spectra of An, AnHe, and $AnHe_2$ in the region of the An 0_0^0 (Figure 2). These spectra show an additive red shift of the 0_0^0 transition upon addition of one and two He, and a progression in the An-He stretch (see Table I). From the An-He stretching frequency and anharmonicity, it is possible to estimate the binding energy for the cluster (based on assumed Morse potential) as 100 cm^{-1} ± 50. This calculation is very crude, not only because a Morse potential was assumed, but because small errors in the peak positions of the weakest peaks can lead to large errors in the calculated binding energy. Better estimates are available from the DE data which will be elaborated in the Discussion section.

The assignment of the AnHe and $AnHe_2$ 2-color MS as consisting of a red shifted origin and vdW stretches to the blue is supported by the high resolution DE spectra shown in Fig. 3. As the 0_0^0 of AnHe (and necessarily An and $AnHe_2$) is pumped, the DE spectrum shows at least one member of a progression of the vdW stretch in the ground state. The transition shown is I_2^0 and one member in the progression $I_2^0V_x^0$ is clearly identified. If one quantum of the vdW stretch is excited, the progression $I_2^0V_x^1$ is observed with the most prominent feature being $I_2^0V_1^1$ indicating a strong $\Delta V = 0$ propensity rule. The observation that V^1 is nearly identical to V_1 (10.4 cm^{-1} and 9 cm^{-1}, respectively) implies that $I_2^0V_1^1$ is nearly isoenergetic with I_2^0 and indicates that the vdW potential is not essentially different in the ground and excited states.

It is proposed in I that relaxed emission observed while pumping An absorption peaks is actually due to vibrational predissociation of $AnHe_x$. Figure 4 presents strong additional evidence supporting this proposed mechanism. The lower trace shows a portion of the DE spectrum obtained while pumping An $6a_0^1$. The upper trace shows the same spectrum after a small amount of CH_4 has been mixed into the system. Note the dramatic decrease in the relative intensity of the relaxed peaks upon addition of CH_4. Methane competes with He in the formation of vdW complexes. Addition of methane decreases the concentration of $AnHe_x$ and reduces relaxation in the system. Further discussion of the implications of these data for the relaxation mechanisms previously proposed will be presented in the Discussion section.

B. An-CH_4 System

0_0^0 - This transition was studied most extensively because little interference exists in this case from other observable An bands. The well studied hot bands[8] in this region disappear at $P_o \gtrsim 250$ psi. $AnHe_x$ features are greatly reduced due to the presence of CH_4, and the $AnHe_x$ absorption features are confined to the region immediately surrounding and to the blue of the An 0_0^0. Therefore, the observed absorption features in this region are due to $An(CH_4)_x$ species. No species of the form $An(CH_4)_yHe_x$ have been observed.

The region from 0 to -80 cm^{-1} relative to An 0_0^0 is dominated by the $AnCH_4$ species as is clearly shown in Fig. 5. The major features in the FE spectrum (upper trace) are reproduced in the 2-color MS of $AnCH_4$. The spectrum consists of transitions due to the $AnCH_4$ 0_0^0 80 cm^{-1} red shifted from the An 0_0^0 and various vdW motions of the $AnCH_4$ species to the blue of the $AnCH_4$ 0_0^0 (see Table II). The $AnCH_4$ origin consists of three peaks: this triplet structure may arise from three different conformations for the $AnCH_4$ species, or from vdW bending modes built on the $AnCH_4$ 0_0^0. The relative intensities of the three peaks remains constant as the nozzle backing pressure is varied.

The general assignment of the $AnCH_4$ 0_0^0 region is supported by the DE spectra associated with this region. Figure 6 shows a portion of the An 0_0^0 DE spectrum and the DE spectra of various $AnCH_4$ features. For all of the $AnCH_4$ features pumped the dominant emission is isoenergetic with emission from $AnCH_4$ 0_0^0. Apparently, pumping a vdW motion of the $AnCH_4$ results in emission predominantly to the same vdW motion in the ground state. This

interpretation is supported by high resolution DE spectra. Figure 7 presents a small portion of the dispersed emission spectrum associated with pumping the origin region of $AnCH_4$. If the $AnCH_4$ 0^0 state is excited, emission is observed corresponding to the $I_2^0V_0^0$ and $I_2^0V_1^0$ transitions; if the $AnCH_4$ 0^0V^1 state is excited, emission is observed corresponding to the $I_2^0V_1^1$ and $I_2^0V_0^1$ transitions. The relative intensities in the spectra further confirm the $\Delta V=0$ propensity rule previously suggested. These spectra not only support the assignment of the $AnCH_4$ 0_0^0 features, but also show that the feature 24 cm^{-1} blue shifted with respect to the $An(CH_4)$ origin is one quantum of an $AnCH_4$ vdW motion. In addition, the observation that this motion is nearly the same in the ground and excited state (25 cm^{-1} and 24 cm^{-1}, respectively) indicates that An-CH_4 potential surfaces do not differ greatly in the ground and excited states.

The spectral region from -80 cm^{-1} to -160 cm^{-1} relative to the An 0_0^0 is dominated by the $An(CH_4)_2$ species as Fig. 8 indicates. The major features in the FE spectrum in this region (upper trace) are reproduced by 2-color MS obtained by selective observation of the $An(CH_4)_2$ mass channel. The $An(CH_4)_2$ 0_0^0 is red shifted 162 cm^{-1} from the An 0_0^0 and some structure due to vdW bond modes is evident to the blue of the $An(CH_4)_2$ origin. The exception to this assignment is the band at -130 cm^{-1} in the FE spectrum. This feature is not a hot band as it increases rather than decreases with increasing nozzle backing pressure. It is not due to $An(CH_4)_2$ since it doesn't appear in the 2-color MS; it has been assigned to the An_2 species although the appropriate 2-color MS study to confirm this was inconclusive due to poor An_2 signal levels.

The FE spectrum to lower energy than the $An(CH_4)_2$ origin consists of a broad continuum that decreases in intensity to lower energy. Figure 9 shows that $An(CH_4)_x$ species generate a rising intensity background relative to An expanded in pure He. Mass spectra generated by excitation in this region, one of which is shown in Fig. 10, indicate that the absorption intensity in this region is dominated by the $An(CH_4)_3$ and $An(CH_4)_4$ species. This indicates that the spectral shifts of the origins of various clusters is no longer additive for $An(CH_4)_x$ with $x > 3$. The mass spectrum presented in Fig. 10 is obtained by 1-color 2 photon ionization; the intensity in the An, $An(CH_4)$ and $An(CH_4)_2$ mass channels is due to fragmentation. Higher clusters are also observed in this mass spectrum indicating that they too absorb ca. 200 cm^{-1} below the An 0_0^0 transition.

$10b_0^2$, $16a_0^2$ - Figure 11 shows the FE and 2-color MS of $AnCH_4$ associated with the $10b_0^2$ and $16a_0^2$ transitions. The spectral features differ significantly in relative intensities from those observed for the 0_0^0 transition. This is most likely due to the overlap of $AnCH_4$ features associated with $10b^2$ and $16a^2$ as these two transitions are separated by only 7 cm^{-1}. Thus the resulting spectra appear broad. Moreover, spectral intensity due to $An(CH_4)_2$ associated with the $6a_0^1$ transition further hampers a detailed study of the features related to An-CH_4 vdW clusters at $10b^2$ and $16a^2$.

$6a_0^1$ - Figure 12 presented the FE and 2-color mass spectra of $AnCH_4$ associated with the An $6a_0^1$ transition. The spectra of $AnCH_4$ for this transition are virtually identical to those observed for the 0_0^0 transition with respect to relative intensities and shifts. Notice again the good

correlation between the FE spectra and the 2-color MS. The -80 cm^{-1} band is the most intense feature in both spectra and is thus assigned as the $AnCH_4$ $6a_0^1$ and the blue shifted bands relative to $AnCH_4$ $6a_0^1$ are its associated vdW modes. The relative energy of various bands are tabulated in Table II.

Presumably, the $An(CH_4)_2$ $6a_0^1$ is red shifted 160 cm^{-1} from An $6a_0^1$ as is the case for this species near the origin transition. However, this feature would be buried in the congestion associated with the $10b_0^2$ and $16a_0^2$ transitions and could not be unambiguously assigned.

The DE spectrum of $AnCH_4$ asociated with the $6a^1$ state shows broad features with high background. The estimated intensity of the emission features is at least five times weaker than expected. It should be emphasized that the DE spectrum of the An monomer of this transition shows no broadening. Fig. 13 presents a portion of the DE spectra generated by pumping An $6a_0^1$ (lower trace) and $An(CH_4)$ $6a_0^1$. This broadening is most likely due to IVR, as will be discussed more fully in the next section.

Higher Vibronic Transitions - Figures 14, 15 and 16 show FE spectra of the An-CH_4 system (upper traces) compared to some spectra with An-He only. Although this region is highly congested, careful examination of the spectra reveals absorption features due to $An(CH_4)_x$. Transitions 15_0^2, I_0^2 and 1_0^1 of $AnCH_4$ can be distinguished and their spectral red shifts from their An counterparts are 75 cm^{-1}, 77 cm^{-1} and 82 cm^{-1}, respectively. The 15_0^2 and I_0^2 transitions of $An(CH_4)_2$ can also be identified with red shifts of 152 cm^{-1} and 153 cm^{-1}, respectively. No 2-color MS are observed in this region due to vibrational predissociation (VP) of the vdW species. Dispersed emission from the $AnCH_4$ 15_0^2 (Fig. 17) shows sharp features from the An 0^0 level only, thus confirming that the $AnCH_4$ 15^2 level undergoes rapid VP. Emission from I^2 and 1^1 levels evidenced similar results.

IV. DISCUSSION

In this section, discussion will focus both on the physical properties of the clusters and on the relaxation mechanisms of the excited species. The An-He system will be discussed first, followed by the An-CH_4 system.

An-He System

Two central questions concerning the physical properties of An-He complexes remain unanswered in the discussion of the An-He system in I: What is the dissociation energy (D_o) of the An-He complex, and what are the geometries of these complexes? The 2-color MS experiment has made it possible to obtain distinct and identifiable absorption spectra of each $AnHe_x$ species individually in the 0_0^0 region (Fig. 2). These spectra, together with the high resolution DF spectra (Fig. 3), have led to an unambiguous assignment of the FF spectra and have shed some light on the questions concerning D_o and geometry.

The dissociation energy of the AnHe complex can be estimated from the vdW stretch progression observed in the 2-color MS spectrum (Fig. 2). The calculation using this progression and assuming a Morse potential gives a value for D_o of about 100 cm^{-1}. However, this calculation is only an estimate. Because only a few peaks are intense enough to be identified clearly, and the anharmonicity is small, errors in the measurement of the peak positions can make a tremendous difference in the calculated D_o. Random error of 1 cm^{-1} in the measurement of the spectrum can give an error in D_o of ± 50 cm^{-1}. Also, the Morse potential is a good description of a potential well only near the bottom of the well. The third peak in the progression is already a quarter of the way up the potential well. Using a Morse potential in this case could underestimate D_o significantly.

In paper I, several mechanisms were proposed which could lead to the fluorescence observed upon exciting a vdW feature. As was suggested previously and is stated more definitively below, an excited $AnHe_x$ can evidence two relaxation pathways under the conditions in the beam: fluorescence to the ground state (CVLF), predominately to levels with the same quanta of the vdW stretching vibration as in the excited state, or vibrational predissociation (VP) followed by monomer An fluorescence. Assuming that only these two mechanisms are important under our experimental conditions, it is possible to reexamine some of the DE data and get a better estimate of D_o. The lower trace of Fig. 4 shows part of the DE spectrum obtained by pumping An $6a_0^1$ (and necessarily AnHe $6a_0^1$ and $AnHe_2$ $6a_0^1$). Several relaxation peaks are evident in this spectrum, most notably I_1^1 and $I_1^1 6a_1^0$: these peaks are due to VP of AnHe and $AnHe_2$. Since the difference in energy between the $6a^1$ and I^1 levels in An is 155 cm^{-1}, D_o for AnHe (the dominate vdW species) must be less than 155 cm^{-1}.

With the help of additional assumptions, further examination of the $6a_0^1$ DE spectrum can also yield an estimate of the lower limit to D_o. A small emission peak in this spectrum, identifiable as $10b_2^2$, is observable, although it is much weaker than I_1^1. One possible explanation for the poor intensity of $10b_2^2$ is that the oscillator strength of the transition is much smaller than for I_1^1. However, DE spectra from $10b^2$ presented in I show the $10b_2^2$ peak to be quite strong. The only direct comparison of I_1^1 and $10b_2^2$ intensity is found in the 1_0^1 DE spectrum,[6] for which both the I_1^1 and $10b_2^2$ peaks, arising from $An(He)_x$ VP, are very weak due to the large

difference in energy between I^1 and $10b^2$ and the much higher 1^1 level. Nevertheless, considering the data in I it would seem safe to assume that the oscillator strengths of I_1^1 and $10b_2^2$ are comparable (within a factor of ~2.)

Assuming that I_1^1 and $10b_2^2$ have comparable oscillator strengths, the only explanation for the small intensity of the $10b_2^2$ transition in the $6a_0^1$ DE spectrum is that the energy gap between $6a^1$ and $10b^2$ is not sufficient to break the AnHe bond. This leads to a lower limit for D_o of 144 cm^{-1}.

If AnHe were the only vdW species in the beam and the An-He D_o = 150 cm^{-1}, one would predict no intensity for the $10b_2^2$ transition in the AnHe $6a_0^1$ DE spectrum. However, several situations could produce a small amount of intensity for $10b_2^2$ in our system. One explanation for this intensity is that D_o for the first He from $AnHe_x$ ($x \geq 2$) is less than 144 cm^{-1}. Since the concentration of $AnHe_x$ is much less than AnHe, the $AnHe_x$ VP peaks would be of much less intensity than those due to VP of AnHe. Another explanation is that the AnHe D_o is very close to 144 cm^{-1} and some VP to $10b^2$ is seen due to the contribution of a small amount of rotational energy. Finally, AnHe may undergo IVR as the An-CH_4 system can. One would expect such emission to be weak and broad. All of these explanations for the observed $10b_2^2$ intensity are consistent with $D_o > 144$ cm^{-1} for AnHe.

It is not possible to arrive at a definitive description of the geometry of the An-He vdW species without higher resolution spectra which show resolved rotational structure. However, some geometry information can be gleaned from the existing data. The 2-color MS (Fig. 2) show a nearly additive spectral red shift for the AnHe 0_0^0 and $AnHe_2$ 0_0^0 peaks. This probably indicates that

the He atoms are adding to two nearly equivalent positions on the An. It is easy to envision only one way to put two and only two equivalent He atoms on An; they must occupy the positions above and below the aromatic ring in a manner analogous to that suggested for tetrazine-He vdW species.[9] This is consistent with the observed red shift of the clusters. He atoms above and below the ring should be more tightly bound in the excited state than in the ground state of An.

The addition of a third He to produce a broad absorption spectrum with a non-additive shift is consistent with the addition of the He to a non-localized, non-ring position, perhaps near the NH_2 group. Larger clusters ($AnHe_x$, $x > 3$) are also observed by 1-color MS to absorb in the same region as the $AnHe_3$ clusters. The absorption profile for a system of $AnHe_x$ in which $x \geq 3$, with its limiting value of solvent shift, begins to resemble that of a solution.

Several questions concerning the possible pathways which an excited $AnHe_x$ can take were raised previously in I. The conclusions reached in that work, some of which were tentative, were as follows: an An^* molecule can only fluoresce from the vibronic level that was excited (SVLF); an $AnHe_x^*$ can fluoresce to levels in the ground state with the same quanta of vdW vibrations as in the excited state (SVLF, $\Delta V = 0$); and an $AnHe_x^*$ can VP generating An^* which can fluoresce from a level lower than the one pumped. Mechanisms involving collisions were effectively ruled out as significantly contributing to the relaxation for the beam conditions in our system.

Information presented in this paper strengthens these conclusions. Collisions are further shown not to be important under these beam conditions by

the data presented in Figure 4. Addition of CH_4 is observed to reduce the concentration of $AnHe_x$ species and $An(CH_4)_x$ species do not yield relaxed An emission when An absorption bands are excited. Since reducing the $AnHe_x$ concentration reduces the relaxation, it follows that the relaxation seen when An absorption bands are excited (as well as underlying $AnHe_x$ absorption bands) is associated with VP of the $AnHe_x$ species.

Among other mechanisms, the SVLF of $AnHe_x$ species with a $\Delta V = 0$ propensity rule was proposed to explain the monomer-like emission found by exciting $AnHe_x$ absorption features around the An 0_0^0 transition. Figure 3 demonstrates that $AnHe_x$ species in this region are indeed emitting to produce predominantly monomer-like emission. Furthermore, the lower trace in Fig. 3 emphasizes that if vdW stretches are excited, the fluorescence obeys a $\Delta V = 0$ propensity rule. This information, plus the deduced D_o, indicates that only SVLF with $\Delta V = 0$ is occurring to any great extent from vibronic levels of $AnHe_x$ with insufficent vibrational energy to undergo VP.

An-CH_4 System

The principle observations for the An-He system are applicable to the An-CH_4 system with some modification. The $AnCH_4$ 0_0^0 and $An(CH_4)_2$ 0_0^0 show additive spectral red shifts relative to the An 0_0^0, although the shifts are much greater than for $AnHe_x$, due to the larger polarizability of CH_4. Addition of a third CH_4 produces broad, featureless absorption indicating that, while the first two CH_4 groups add to equivalent positions on the An (above and below the aromatic ring) the third CH_4 adds to an inequivalent, less localized position. These observations are qualitatively similar to those made for the An-He system.

Perhaps the most striking difference between the An-CH_4 and An-He systems is the observation of extensive IVR in the An-CH_4 system. This process will be discussed in detail following a discussion of the physical properties of the An-CH_4 clusters.

As can be seen in Figs. 4, 5, and 8. the regions in which $AnCH_4$ and $An(CH_4)_2$ show significant resolved absorption are well separated. $AnCH_4$ absorption features appear in the region -80 cm^{-1} to 0 cm^{-1} relative to An 0_0^0, while $An(CH_4)_2$ absorbed in the region -160 cm^{-1} to -80 cm^{-1}. The $AnCH_4$ 0_0^0 seems to be composed of three overlapping peaks (Fig. 5). Since all three features appear in the $AnCH_4$ 2-color MS and the relative intensities are independent of backing pressure, all three must be due to the $AnCH_4$ complex. Two assignments for these features are possible: the $AnCH_4$ 0_0^0 peak could be split due to the existence of three $AnCH_4$ species, and one or two of the peaks could be vdW bending modes. At this time these two assignments cannot be distinguished.

The general appearance of the An-CH_4 absorption spectra evidences much more congestion than is observed in the An-He spectra. The appearance of possibly three conformers each with a different stretching mode, plus the possibility that bending modes may be contributing intensity, can account for the congestion. The congestion increases as more CH_4 molecules are added. One can easily envision the absorption spectrum transforming to a broad, structureless feature with a center somewhere to the red of $An(CH_4)_2$ 0_0^0 in the region in which a large number of clusters $(An(CH_4)_x$ where $x \geq 3)$ are observed to absorb. This might well lead to a description of an An-CH_4 solvation spectrum. Cryogenic solution spectra of An-CH_4 were not obtainable

due to low solubility; however, one can predict by comparison with benzene and toluene solution data that an An-CH_4 solution would give an An 0_0^0 red shift of ca. 250 cm^{-1}.[10]

Higher transitions exhibit similar spectral shifts and patterns in the vdW vibrations. These absorption patterns are identifiable in the $AnCH_4$ $6a_0^1$ region (Fig. 12) for which they are free of congestion from other vibronic bands. The emission spectra of higher vibronic bands can give an estimate of the dissociation energy of the $AnCH_4$ complex. Emission from $AnCH_4$ 15^2 or higher levels evidence strong, sharp emission from the An 0^0 level as given in Fig. 17. This demonstrates that 699 cm^{-1} is sufficient to cause VP of the An-CH_4 bond and sets a firm upper limit to the dissociation energy.

Emission from the $AnCH_4$ $6a^1$ level is broad and featureless and shifted 80 cm^{-1} to the red of An $6a^1$ emission. Time of flight mass spectra taken with $6a^1$ as the intermediate level demonstrate that excitation to the $AnCH_4$ $6a^1$ level does not lead to VP and therefore $D_0 > 498$ cm^{-1}. The emission from $AnCH_4$ $10b^2$ and $16a^2$ is similar in appearance although much weaker than the $AnCH_4$ $6a^1$ emission, as is expected.

The broad and featureless appearance of the $AnCH_4$ $6a_0^1$ emission (Fig. 13) is attributed to IVR of the $AnCH_4$ $6a^1$ level before emission. The IVR process may arise in the An-CH_4 system and not in the An monomer due to the increased density of states afforded by the creation of various vdW modes. The largest features in the $AnCH_4$ $6a_0^1$ emission spectrum are red shifted ~80 cm^{-1} from the An $6a_0^1$ spectrum. However, in the $AnCH_4$ $6a_0^1r_2^0$ emission peak (Fig. 13), for example, substantial intensity is present to the red of the major peak. This intensity may be due to IVR peaks such as $10b_1^1$, $10b_2^2$,

15_1^1, or it could be due to emission from several vdW modes built on different An vibronic levels populated by the IVR process. In any case, the general appearance of the spectrum leads to the conclusion that IVR is important at the $AnCH_4$ $6a^1$ level, although some SVLF may be found within the IVR related emission background.

Although it is impossible to set quantitative rates for the IVR or VP processes from the observed spectra, it is possible to compare qualitatively the rates for IVR and VP with the fluorescence rate. The rate of VP is fast compared to the fluorescence lifetime (5 ns) since the VP process is complete within this period. Also, an upper limit to the rate of VP can be estimated from the linewidth of the transitions to states more than 699 cm^{-1} above CH_4 0_0^0. Since the linewidths do not change noticeably between transitions to states that undergo VP and those that do not, the lines are inhomogeneously broadened and the rate of VP must be much slower than the linewidth estimated lifetime of 5 ps would indicate. The rate of IVR must be much slower than the rate of VP since the DE from $AnCH_4$ 15^2 and higher levels does not evidence any IVR related broad emission. It can also be concluded that the rate of IVR is somewhat faster than the rate of fluorescence since the $AnCH_4$ $6a^1$ emission does not show strong SVLF, although IVR is not a great deal faster than the fluorescence rate since IVR is not complete before the complex fluoresces. One can therefore express qualitatively the relative rates as follows: fluorescence (10^9/sec) < IVR << VP << 10^{12}/sec.

The IVP rates have been studied in other systems. In the tetrazine-argon (Tet-Ar) system[12] the rate of IVR is comparable to the rate of VP. Pumping an excited vibronic level results in SVLF, sharp, relaxed emission due to VP,

and broad, symmetric emission peaks due to IVR. The fluorescence intensity associated with each of these processes is compared to find the relative rates for the different processes. In the Tet-Ar system, the SVLF rate is fastest, with the IVR and VP rates nearly the same for many levels. It appears that the rate of IVR for a system is primarily governed by the density of states in the system.

In light of the above discussion concerning the IVR process in An-CH_4 clusters, it is possible to draw another parallel between vdW clusters and liquid state behavior. For liquids, in general, what emission does occur almost invariably arises from the lowest vibrational level of the first excited state of a given spin manifold.[13] Moreover, the emission from liquids tends to be broad and is often temperature dependent. Most of these trends are distinctly seen in $An(CH_4)_x$ vdW clusters. As cluster binding energy becomes larger (better solvents) and presumably as cluster size increases, IVR becomes a more dominant process. As IVR becomes faster, thermal equilibrium can be established more readily in the excited state for both clusters and real solutions. Indeed, the excited state kinetics observed in the liquid can be explained by a rapid IVR process which arises, not from a perturbation of solute levels per se, but from a substantial increase in the density of states experienced by the solute and associated with local solute/solvent clusters or solvent cage formation. In solution, such clusters are necessarily of a highly dynamic nature but they may live for a time long compared to the cluster VP and IVR times.

V. CONCLUSIONS

The 2-color MS technique has allowed a much greater understanding of both the physical properties and the relaxation processes in the An-He and An-CH_4 systems. The essential general conclusions which follow for the vdW cluster systems are enumerated below.

1. The AnHe 0_0^0 and $AnHe_2$ 0_0^0 evidence additive red shifts relative to An 0_0^0, whereas the $AnHe_3$ 0_0^0 is broad and exhibits a non-additive spectral shift. Larger clusters (x>3) absorb in the region of $AnHe_3$ indicating a limiting value for a cluster (solvation or cage) shift.

2. Both An-He and An-CH_4 vdW species seem to show a strong preference for binding the ligand above and below the An aromatic ring.

3. An-He vdW stretching modes are clearly evident and can be used to estimate the An-He dissociation energy as 100 ± 50 cm^{-1}. DE experiments can be used to bracket the dissociation energy at 144 $cm^{-1} < D_o < 155\ cm^{-1}$.

4. Excited $AnHe_x$ clusters undergo VP if sufficient vibrational energy is present, otherwise, they SVLF with a strong $\Delta V = 0$ propensity rule. Excited An can only SVLF under the experimental conditions of the present study.

5. $AnCH_4$ and $An(CH_4)_2$ vibronic bands show additive spectral red shifts of 80 and 160 cm^{-1}, respectively. The $An(CH_4)_3$ 0_0^0 is broad and exhibits a non-additive spectral shift. Larger clusters of An-CH_4 absorb in the same region as $An(CH_4)_3$, indicating that the limiting value for a cluster (solvation or cage) shift is produced by three solvent molecules for both He and CH_4.

6. The $AnCH_4$ 0_0^0 and 6_0^1 are split into 3 peaks due to the presence of more than one conformer, or the presence of vdW bending modes or both.

7. The dissociation energy of $AnCH_4$ is between 498 cm^{-1} and 699 cm^{-1}.

8. If $AnCH_4$ is excited with $\leq$498 cm^{-1} of excess vibrational energy, the emission is broadened by IVR.

9. The rate of IVR from the $AnCH_4$ $6a^1$ level is somewhat faster than fluorescence and substantially slower than the rate of VP.

10. The vdW potentials for both the An-He and An-CH_4 systems are similar in the ground and excited states of a given species.

Some similarities can be pointed out between solution phenomena for molecules like An in simple cryogenic molecular hydrocarbon liquids and gas phase vdW clusters for the same solute/solvent sets. The two most striking similarities are the apparent importance of the IVR process for excited state kinetics in both clusters and solutions, and the limiting of the cluster (red) shift at roughly three solvent molecules at a value similar to the solution value.

Future studies are aimed at obtaining high resolution FE and two-color MS of the different clusters in order to gain more information about goemetry. Also, other systems are being explored to answer questions about the IVR process, and to explore the relationship between the physical properties of vdW species and cryogenic solution spectra.

REFERENCES

1. See for example:

   D.H. Levy, L. Wharton and R.E. Smalley, Chemical and Biochemical Applications of Lasers, Vol II, pp. 1-41 (Academic Press, New York, 1977).

2. See for example:

   A. Amirav, U. Even and J. Jortner, J. Chem. Phys. 75, 2489 (1981).

3. J.E. Kenny, K.E. Johnson, W. Sharfin and D.H. Levy, J. Chem. Phys. 72, 1109 (1980).

4. J.H. Brophy and C.T Rettner, Chem. Phys. Lett. 67, 351 (1979).

5. M.A. Duncan, T.G. Dietz and R.E. Smalley, J. Chem. Phys. 75, 2118 (1981).

6. E.R. Bernstein, K. Law and Mark Schauer, J. Chem. Phys., in press.

7. K.M. Swift, Ph.D. Thesis "Two-Photon Spectroscopy of Pyrazine, s-Triazine and Osmium Tetroxide", Colorado State University (1981).

8. J.C.D. Brand, D.R. Williams and T.J. Cook, J. Molec. Spec. 20, 359 (1966).

9. R.E. Smalley, L. Wharton, D.H. Levy, and D.W. Chandler, J. Chem. Phys. 68, 2487 (1978).

10. E.R. Bernstein, K. Law and Mark Schauer, unpublished result.

11. R.E. Smmaley, J. Phys. Chem. 86, 3504 (1982).

12. D.V. Brumbaugh, J.E. Kenny and D.H. Levy, J. Chem. Phys. 78, 3415 (1983).

13. F. Li, J. Lee and E.R. Bernstein, J. Phys. Chem. 86, 3606 (1982).

TABLE I

van der Waals modes (in relative cm^{-1}) for $AnHe_x$ 0_0^0 as determined by 2-color MS experiments (Fig. 2). AnHe 0_0^0 and $AnHe_2$ 0_0^0 are red shifted from An 0_0^0 by 1.1 cm^{-1} and 1.9 cm^{-1}, respectively.

	v^1	v^2	v^3
AnHe	10.4	19.7	28.5
$AnHe_2$	9.2	17.3	25.2

TABLE II

$An(CH_4)$ 0_0^0 and $6a_0^1$ features from 2-color MS experiments (see Figs. 5 and 12) (An 0_0^0 at 34031 cm^{-1} and An $6a_0^1$ at 34523 cm^{-1}).

Feature	$An(CH_4)$ 0_0^0	$An(CH_4)$ $6a_0^1$	$An(CH_4)_2$ 0_0^0
	(cm^{-1})	(cm^{-1})	(cm^{-1})
V_0^0 (cm^{-1} relative to An)	0(-80)	0(-80)	0(-160)
Vibrational Modes	9.7	10.5	
	16.9	17.4	
	24	24	
	28.5	29	
	31.7	32.4	
	36.6	37.4	
	47.6	47.6	
	56.7	57.1	
	61.7	61.9	
	65.7	66.2	
	71	70.7	
	72.7	72.5	

FIGURE CAPTIONS

FIGURE 1

One color mass spectra obtained by gating on the labeled mass channel. An was expanded in pure He at 600 psi backing pressure. The frequency scale is relative to An 0_0^0. Fragmentation of clusters due to creating ions with excess vibrational energy causes absorption due to higher clusters to appear in the An and AnHe spectra.

FIGURE 2

2-color MS gated on the labeled species. An was expanded in pure He at P_o = 600 psi. The frequency scale is relative to An 0_0^0. Note that fragmentation has been virtually eliminated. The ionization frequency is 28169 cm^{-1}.

FIGURE 3

One of the DE Peaks obtained by pumping AnHe 0^0 (upper trace) and one quantum of the AnHe stretch. An was expanded with pure He at P_o = 600 psi. The frequency scale is relative to AnHe 0_0^0. For these spectra, the slits are reduced to 5 cm^{-1} resolution. These spectra confirm the assignments of the absorption features being pumped.

FIGURE 4

DE spectra of An $6a_0^1$. The upper trace is obtained from An-He with .2% CH_4 expanded at P_o = 500 psi. The lower spectrum was obtained from An expanded with pure He at P_o = 600 psi. Notice the dramatic decrease in the relaxed peaks, particularly I_1^1 and $I_1^1 6a_1^0$ due to the addition of CH_4.

FIGURE 5

FE (upper trace) and 2-color MS of An-He and .1% CH_4 expansion at P_o = 500 psi. The frequency scale is relative to An 0_0^0 at 34031 cm^{-1}. The 2-color MS experiment involves gating on $AnCH_4$ mass channel. Note that the $AnCH_4$ 2-color experiment reproduces all of the important features in the FE spectrum. The ionization frequency is 28169 cm^{-1}.

FIGURE 6

Part of the DE spectra of An 0_0^0, $AnCH_4$ 0_0^0 and two vdW vibrational peaks built on $AnCH_4$ 0_0^0. An-He was expanded with .1% CH_4 at P_o = 500 psi. Note that the major feature of the $AnCH_4$ spectra are identical and red shifted by ~80 cm^{-1} relative to An 0_0^0.

FIGURE 7

High resolution spectra of the I_2^0 peak in the DE spectrum of $AnCH_4$ 0_0^0 (upper trace), and an $AnCH_4$ vdW motion. An was expanded in He with .1% CH_4 at P_o = 500 psi. Spectral resolution is slit width limited at 10 cm^{-1}. These spectra identify the emitting levels and give the stretching frequency in the ground state as ~25 cm^{-1}.

FIGURE 8

FE spectrum of An expanded He with .2% CH_4 at P_o = 400 psi (upper trace) and 2-color $An(CH_4)_2$ spectrum of An in He and 1.1% CH_4 at P_o = 400 psi. Frequency scale is relative to An 0_0^0. Note that the FE spectrum is nearly identical to the 2-color $An(CH_4)_2$ MS data except for the peak at -130 cm^{-1} which is assigned to An_2.

FIGURE 9

FE spectra of An in He with .1% CH_4 at P_o = 800 psi (upper trace), and An in pure He at P_o = 800 psi. Frequency scale is relative to An 0_0^0. Note the gentle rise in the upper spectrum relative to the An-He baseline. This is due to $An(CH_4)_x$ where $x > 3$.

FIGURE 10

One-color MS of An in He with 1% CH_4 at P_o = 800 psi. The laser wavelength is 2960Å which correspondes to the region in which $An(CH_4)_x$ ($x \geq 3$) absorbs. Mass units are relative to An. Notice that $An(CH_4)_3$ and $An(CH_4)_4$ dominate this region. Although not shown in this figure, $An(CH_4)_x$ species up to $x = 15$ are observed. Peaks corresponding to $An(CH_4)_x$ where $x \leq 2$ are due to fragmentation of larger clusters.

FIGURE 11

FE spectrum near $10b_0^2$ of An in He with .2% CH_4 at 400 psi (upper trace) and 2-color MS of $An.CH_4$ in the $10b_0^2$ region of An in He with .1% CH_4 at P_o = 400 psi (ν_{ion} = 28219 cm^{-1}). Frequency scale is relative to An $10b_0^2$ (34379 cm^{-1}). Note that this region is highly congested with peaks from $10b_0^2$, $16a_0^2$ and $An(CH_4)_2$ $6a_0^1$.

FIGURE 12

FE spectrum of An in He with .2% CH_4 at P_o = 500 psi near the An $6a_0^1$ transition (upper trace) and 2-color MS of $AnCH_4$ for An in He with .1% CH_4 at P_o = 500 psi and ν_I = 28219 cm^{-1}. Frequency scale is relative to An $6a_0^1$ (34523 cm^{-1}). Notice that the FE spectrum in this region is due largely to $AnCH_4$.

FIGURE 13

DE spectrum of $AnCH_4$ $6a_0^1$ (upper trace) and DE spectrum of An $6a_0^1$. Both are obtained for An in He with .2% CH_4 at P_o = 500 psi. Note that $AnCH_4$ $6a_0^1$ emission is broad and featureless and red shifted about 80 cm^{-1} from the An emission.

FIGURE 14

FE spectrum near An 15_0^2 of An in He with .1% CH_4 at P_o = 600 psi (upper trace) and An expanded in pure He at P_o = 600 psi. Although the spectra are complicated by congestion, some $AnCH_4$ peaks are discernable.

FIGURE 15

FE spectra 10-90 cm^{-1} to the red of An 15_0^2 for An in He with .1% CH_4 (upper trace) and An in pure He, both at P_o = 600 psi. Several $AnCH_4$ bands are identifiable.

FIGURE 16

FE spectra 80-160 cm^{-1} to the red of An 15_0^1 for AnHe with .3% CH_4 (upper trace) and An in pure He, both at P_o = 300 psi. Several $An(CH_4)_2$ can be identified.

FIGURE 17

Portions of the DE spectrum of $AnCH_4$ 15_0^2. An was expanded in He with .1% CH_4 at P_o = 600 psi. The observed $AnCH_4$ 15_0^2 emission is identical to An 0_0^0 emission indicating complete and rapid VP at 15_0^2 of $AnCH_4$.

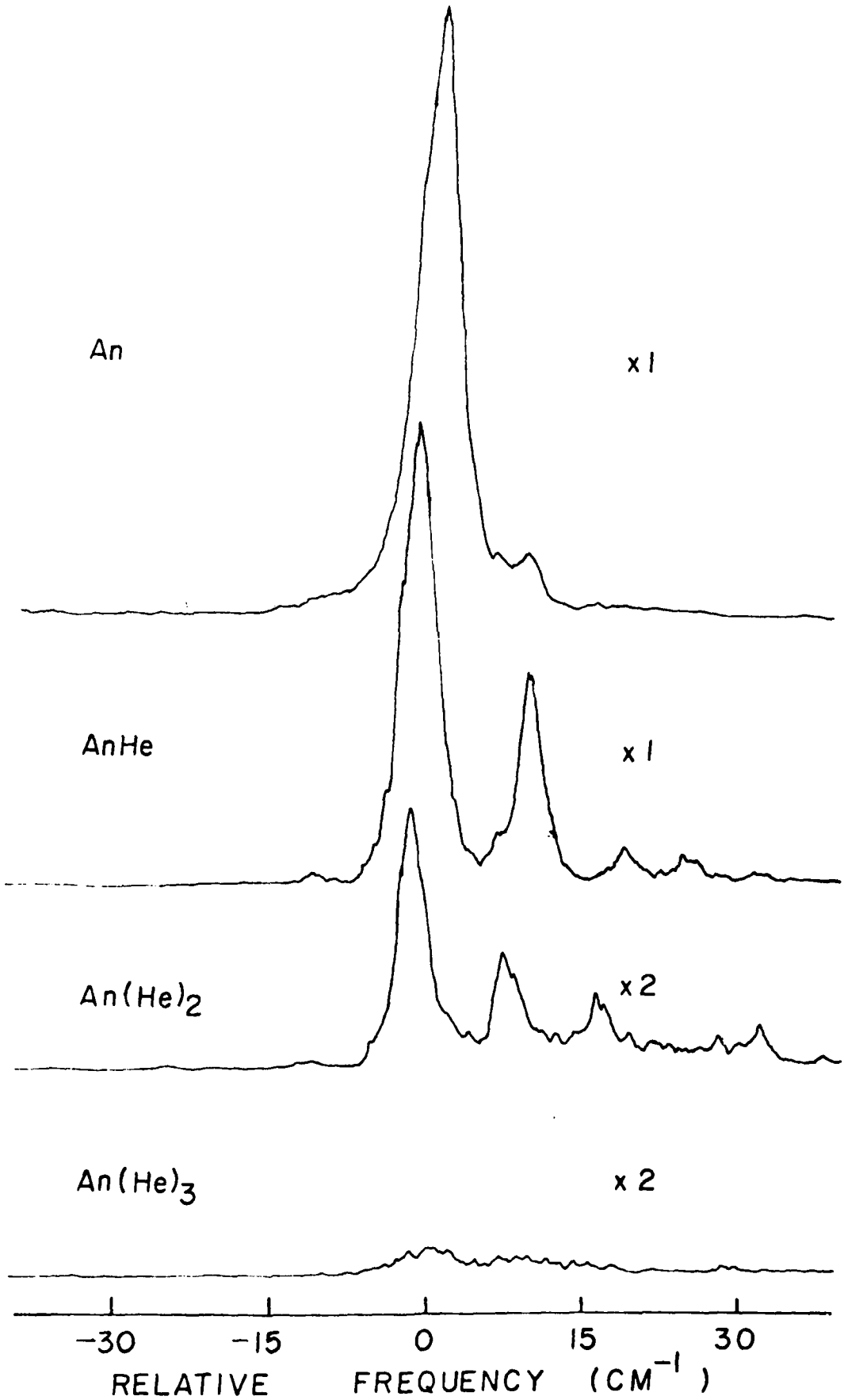
An
x 1
AnHe
x 1
An(He)2
x 2
An(He)3
x 2
−30
−15
0
15
30
RELATIVE FREQUENCY (CM−1)

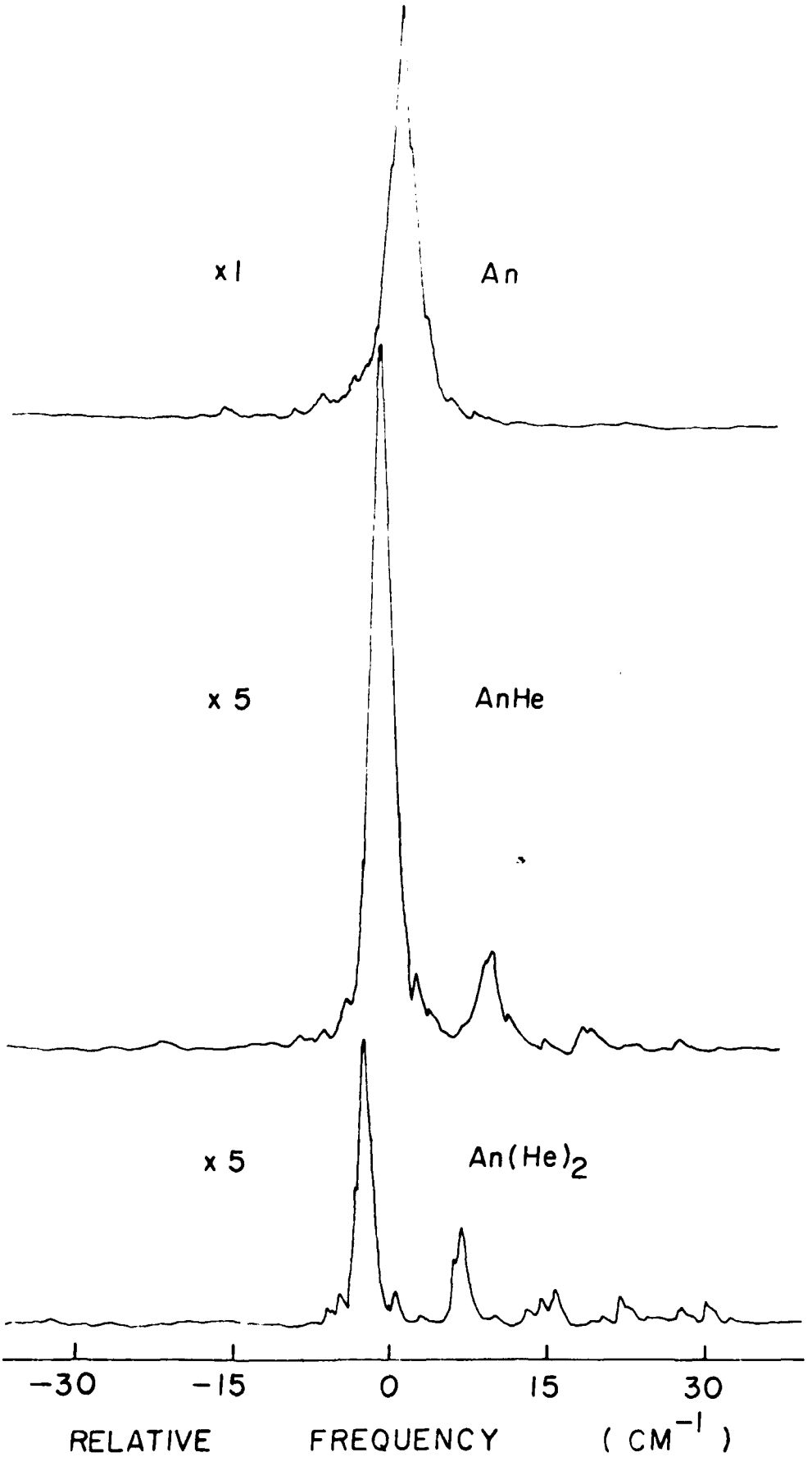
x 1
An
x 5
AnHe
x 5
An(He)2
−30
−15
0
15
30
RELATIVE FREQUENCY (CM−1)

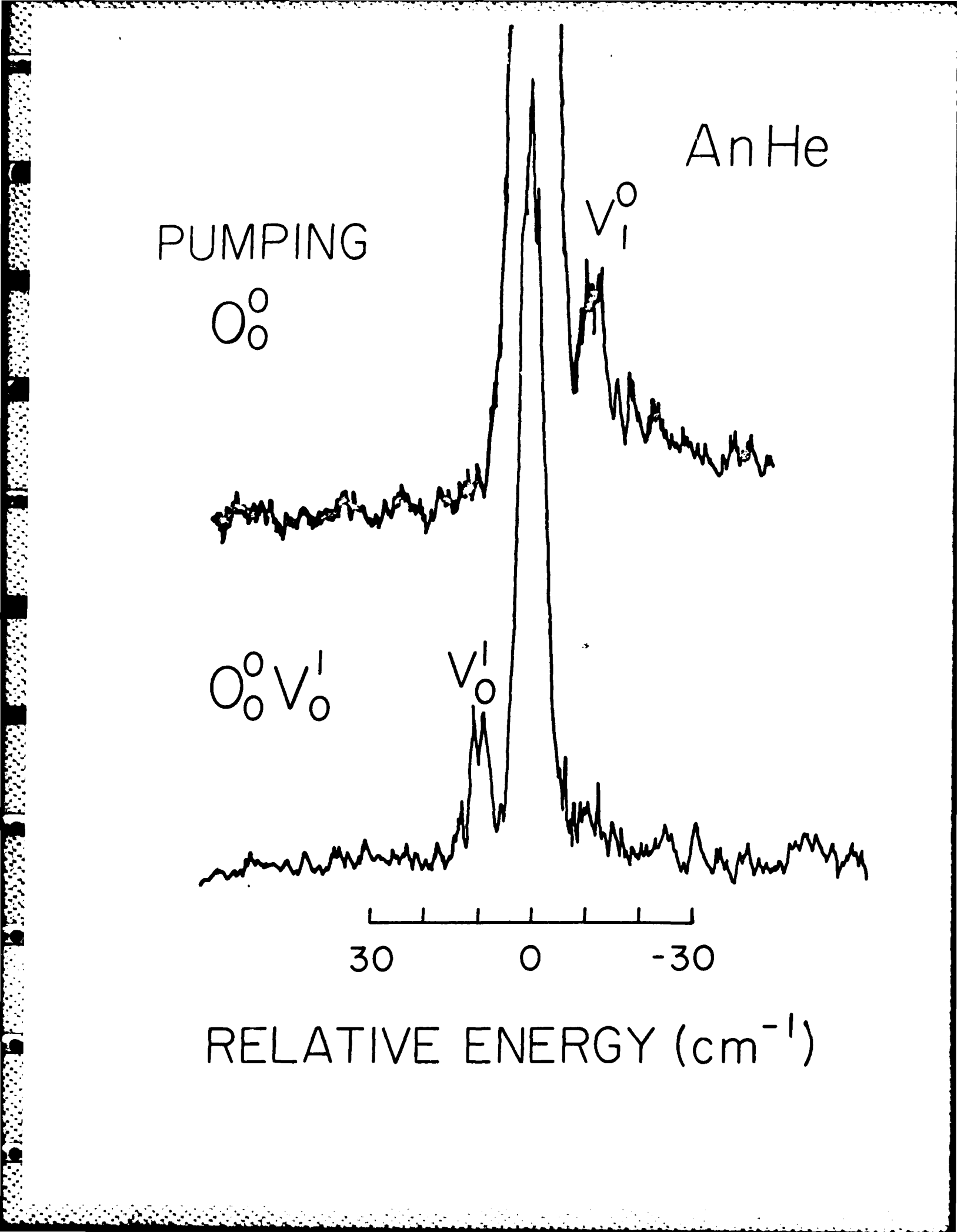
AnHe
PUMPING
O_0^0
V_1^0
$O_0^0 V_0^1$
V_0^1
30
0
-30
RELATIVE ENERGY (cm^{-1})

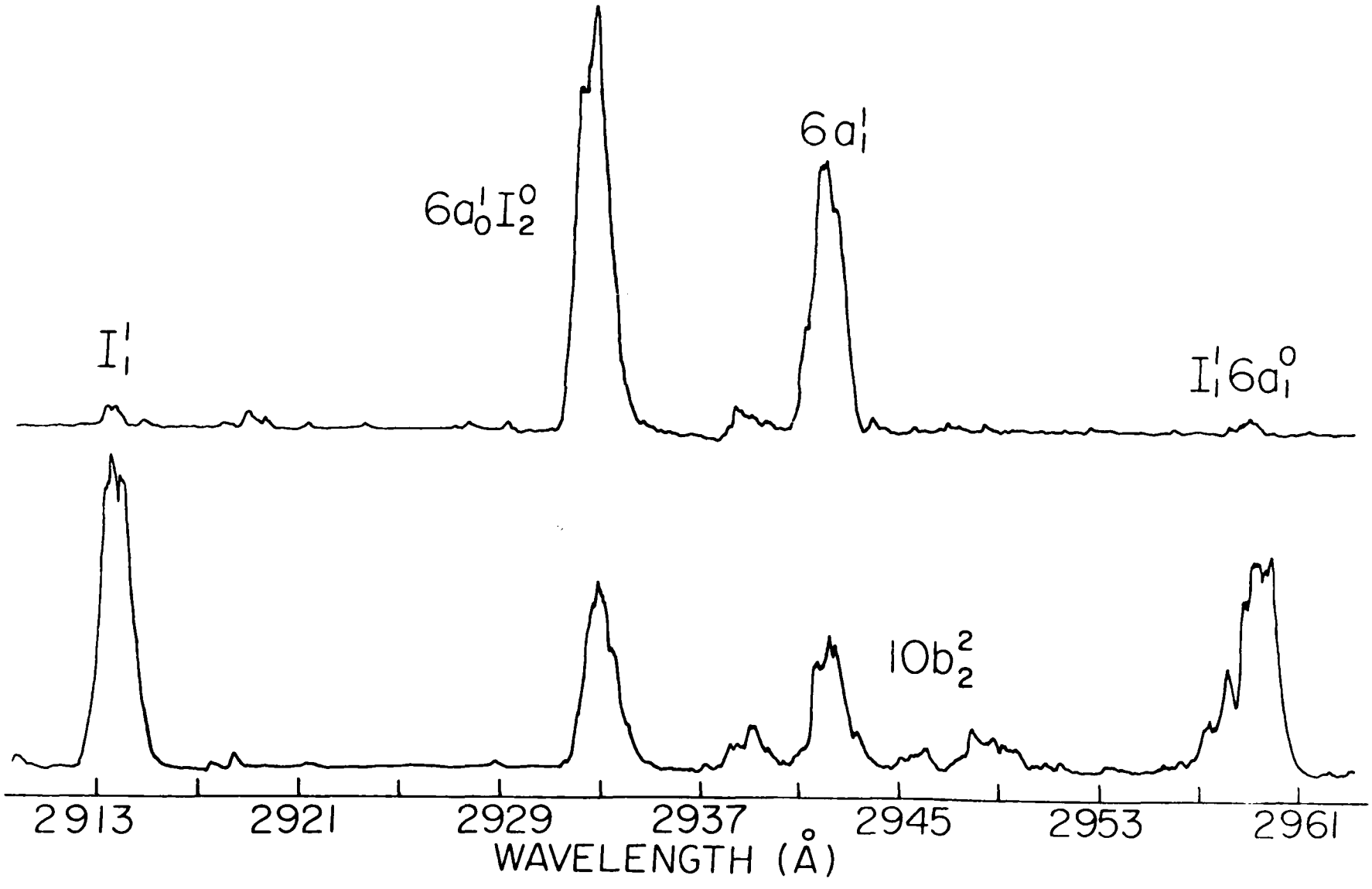
6a'1
6a'0I02
I'1
I'16a01
10b22
2913
2921
2929
2937
2945
2953
2961
WAVELENGTH (Å)

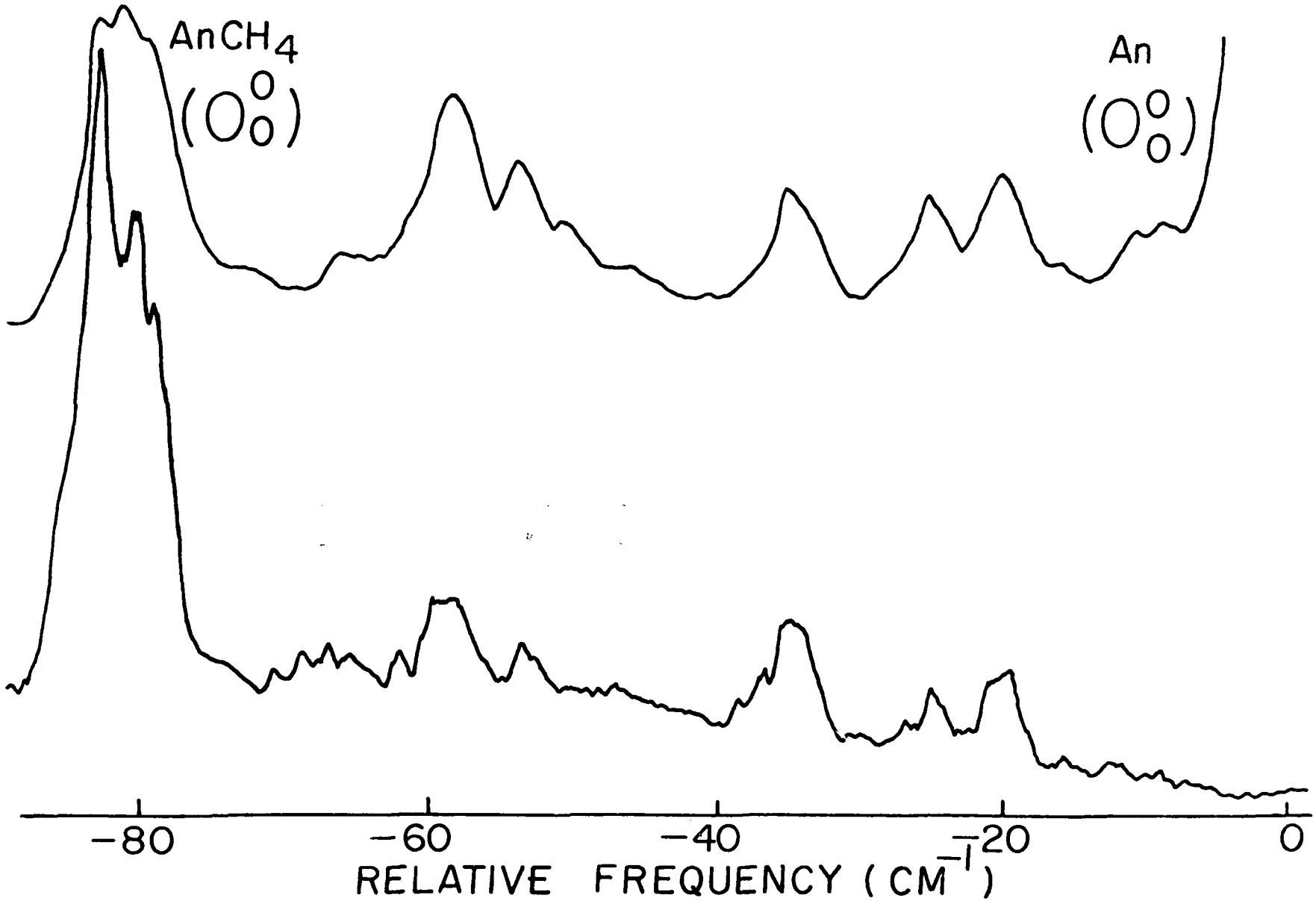
AnCH4
(O00)
An
(O00)
-80
-60
-40
-20
0
RELATIVE FREQUENCY (CM-1)

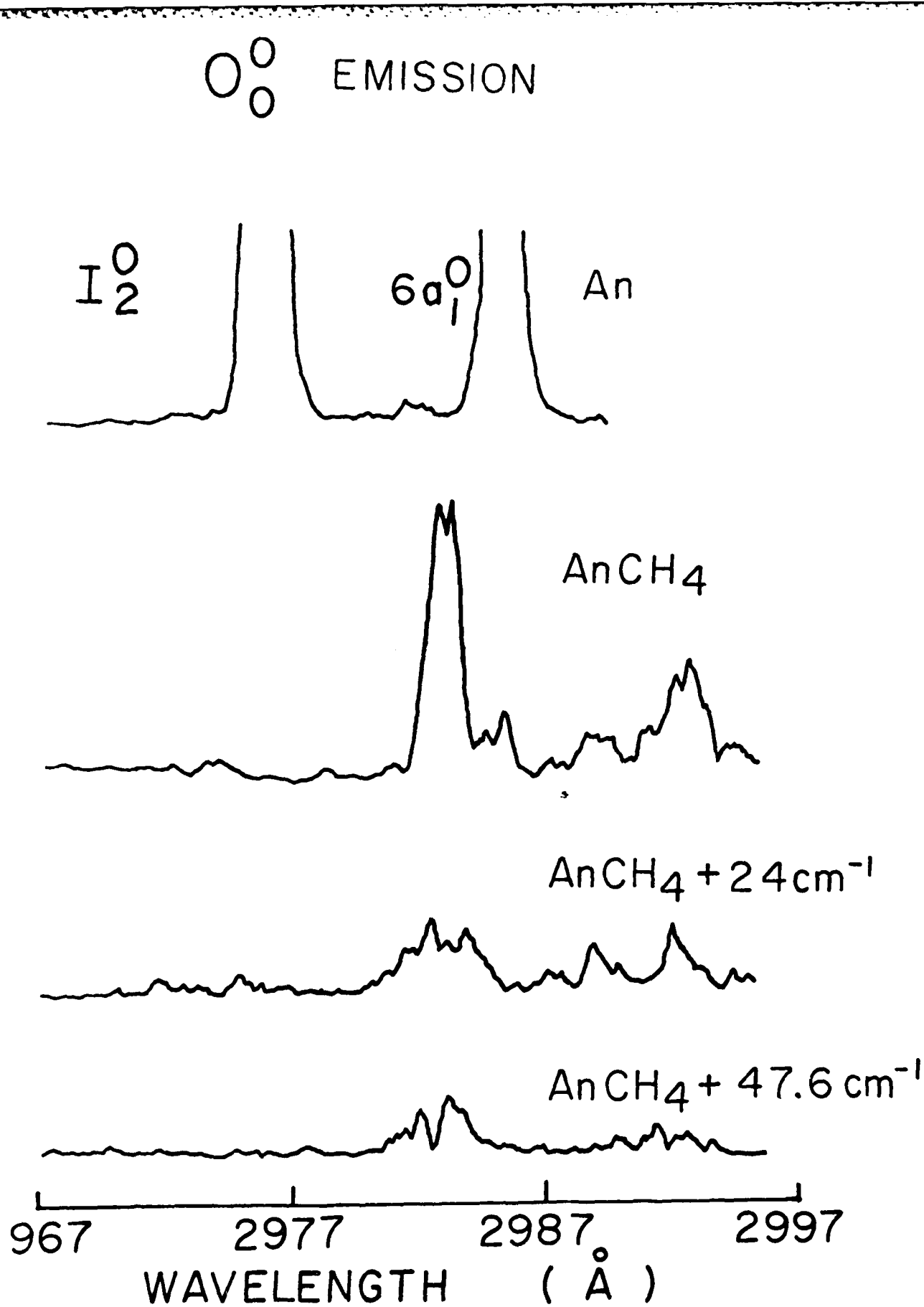
O_0^0 EMISSION
I_2^0
$6a_1^0$
An
$AnCH_4$
$AnCH_4 + 24cm^{-1}$
$AnCH_4 + 47.6\,cm^{-1}$
967
2977
2987
2997
WAVELENGTH (Å)

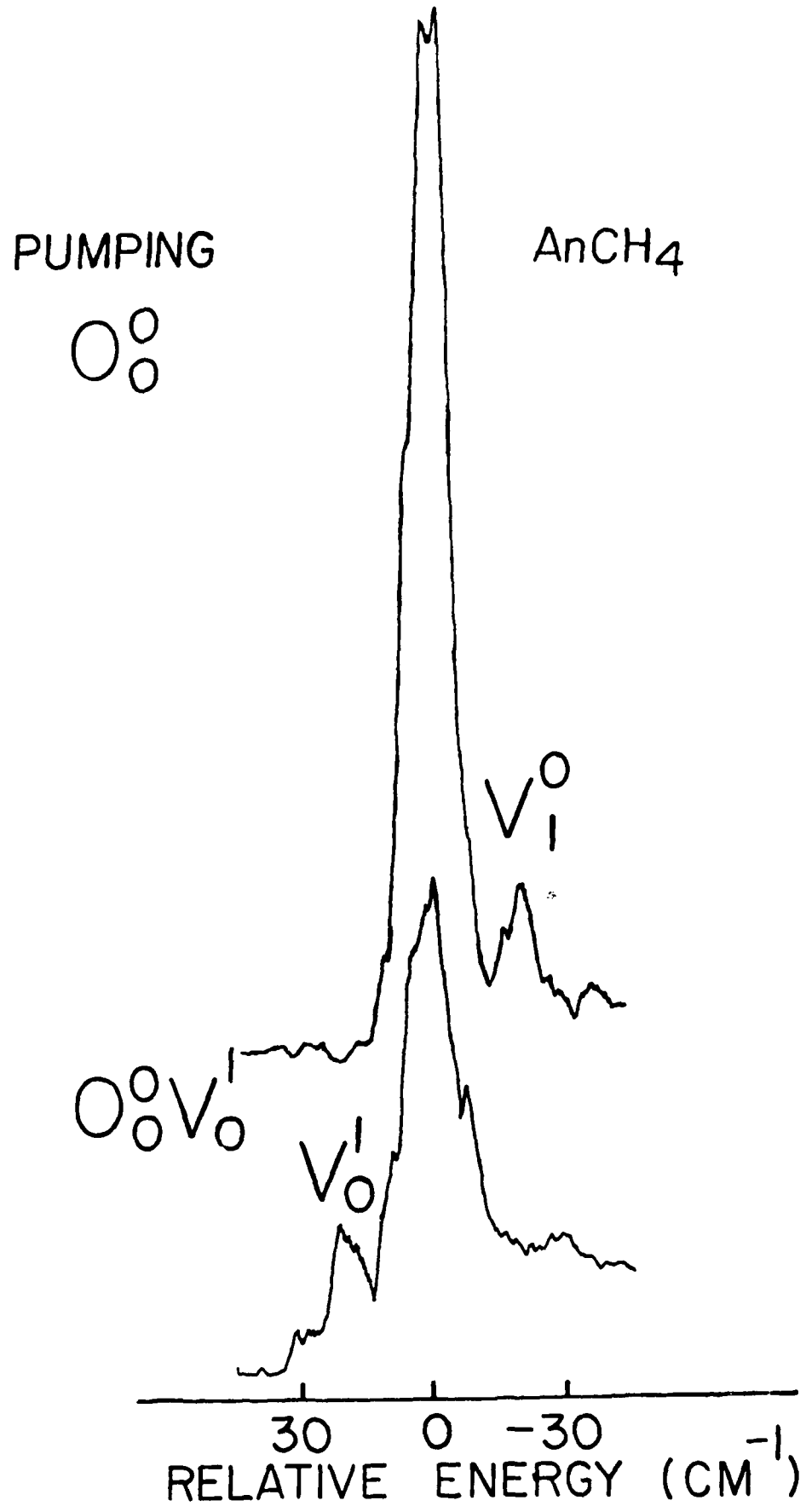
PUMPING
O_0^0
AnCH4
V_1^0
$O_0^0V_0^1$
V_0^1
30
0
-30
RELATIVE ENERGY (CM^{-1})

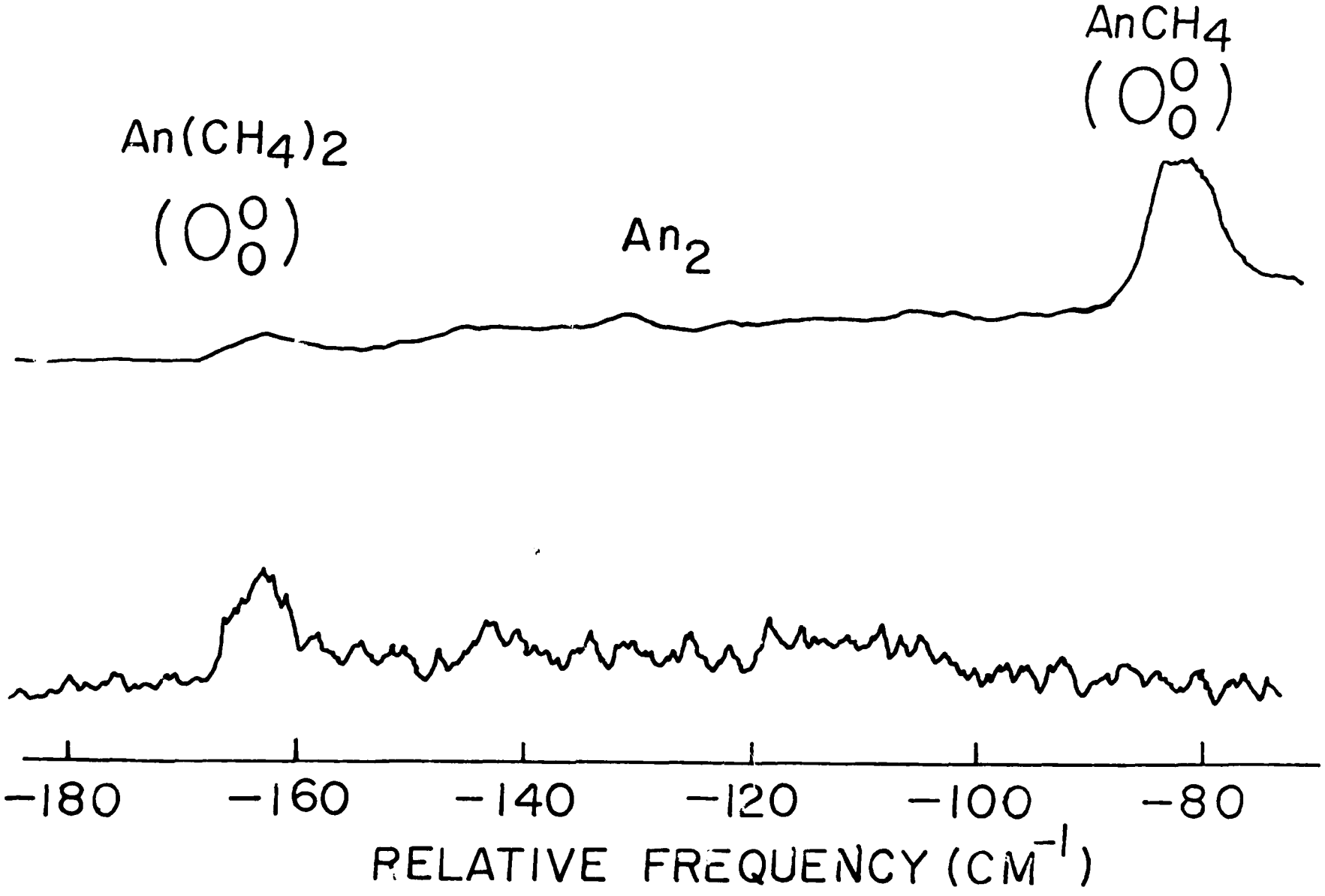
AnCH4
(O00)
An(CH4)2
(O00)
An2
-180
-160
-140
-120
-100
-80
RELATIVE FREQUENCY (CM-1)

O_0^0 $An(CH_4)_x$ $x \geqslant 3$

TOP 0·1% CH_4 + 99·9% He

BOTTOM 100% He

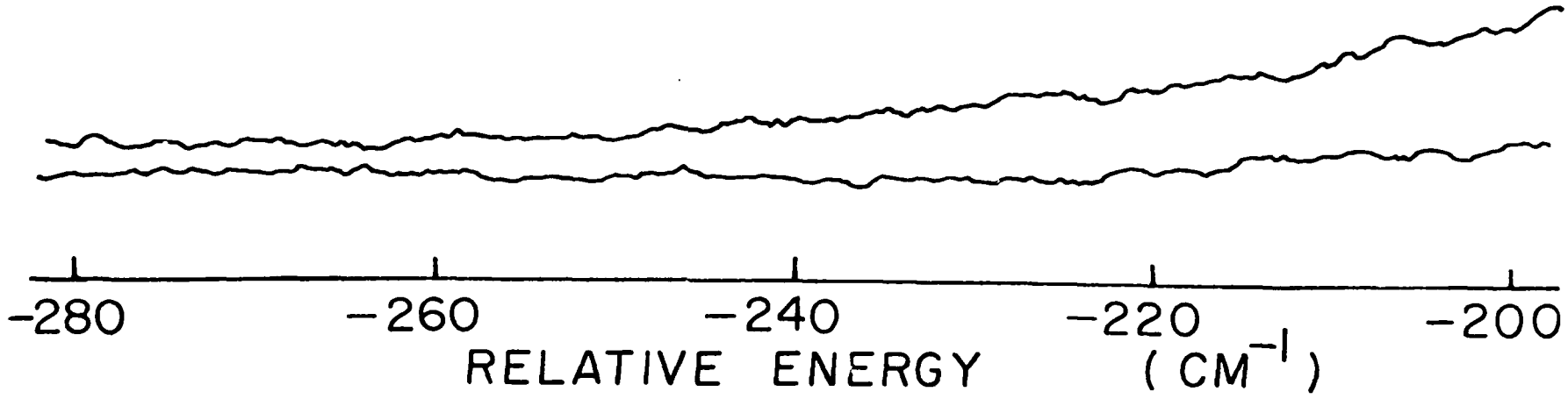

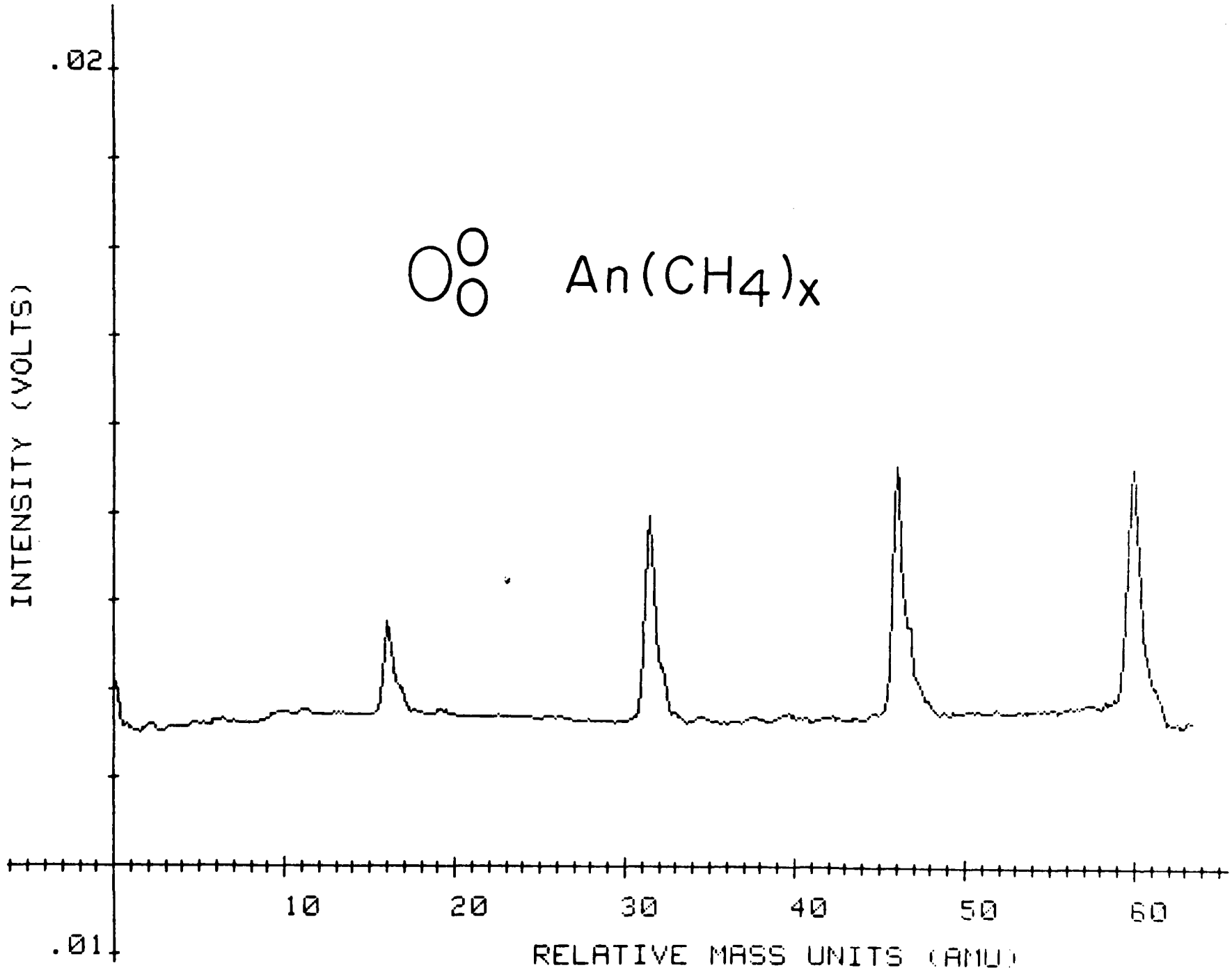
.02
.01
INTENSITY (VOLTS)
O_2^+ $An(CH_4)_x$
10
20
30
40
50
60
RELATIVE MASS UNITS (AMU)

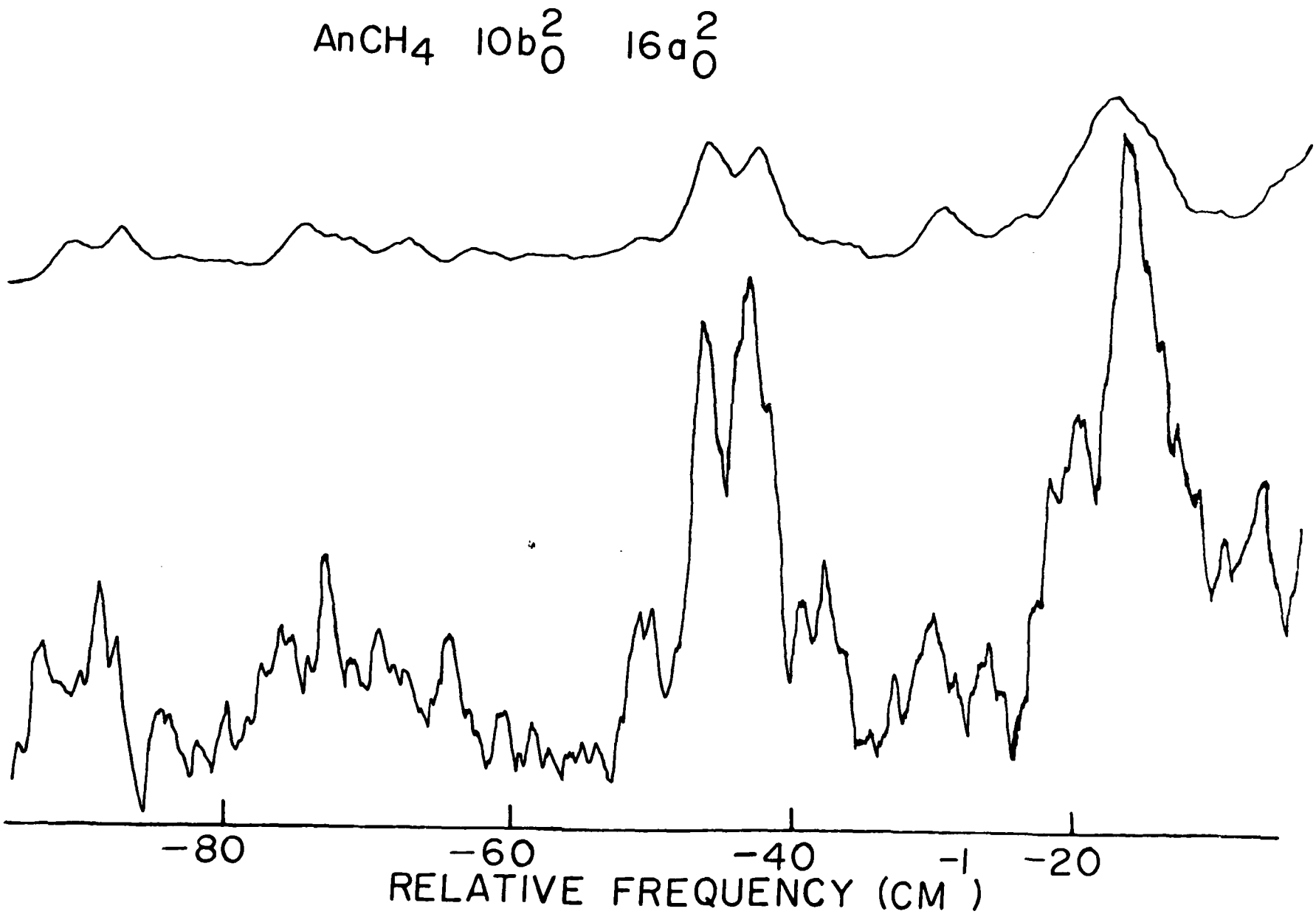
AnCH4 10b2 0 16a2 0
-80
-60
-40
-1
-20
RELATIVE FREQUENCY (CM)

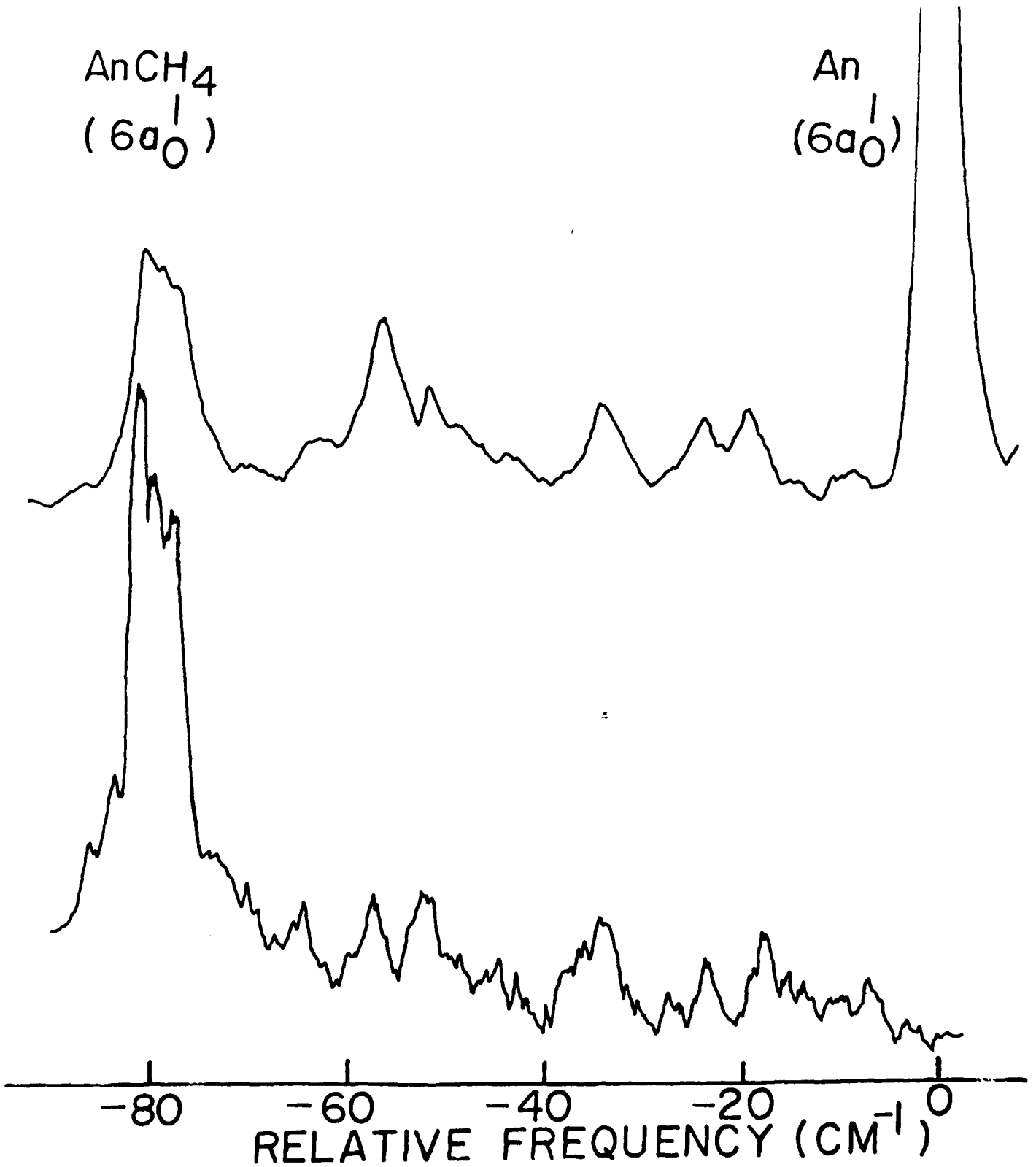
AnCH4
(6a1 0)
An
(6a1 0)
-80
-60
-40
-20
0
RELATIVE FREQUENCY (CM-1)

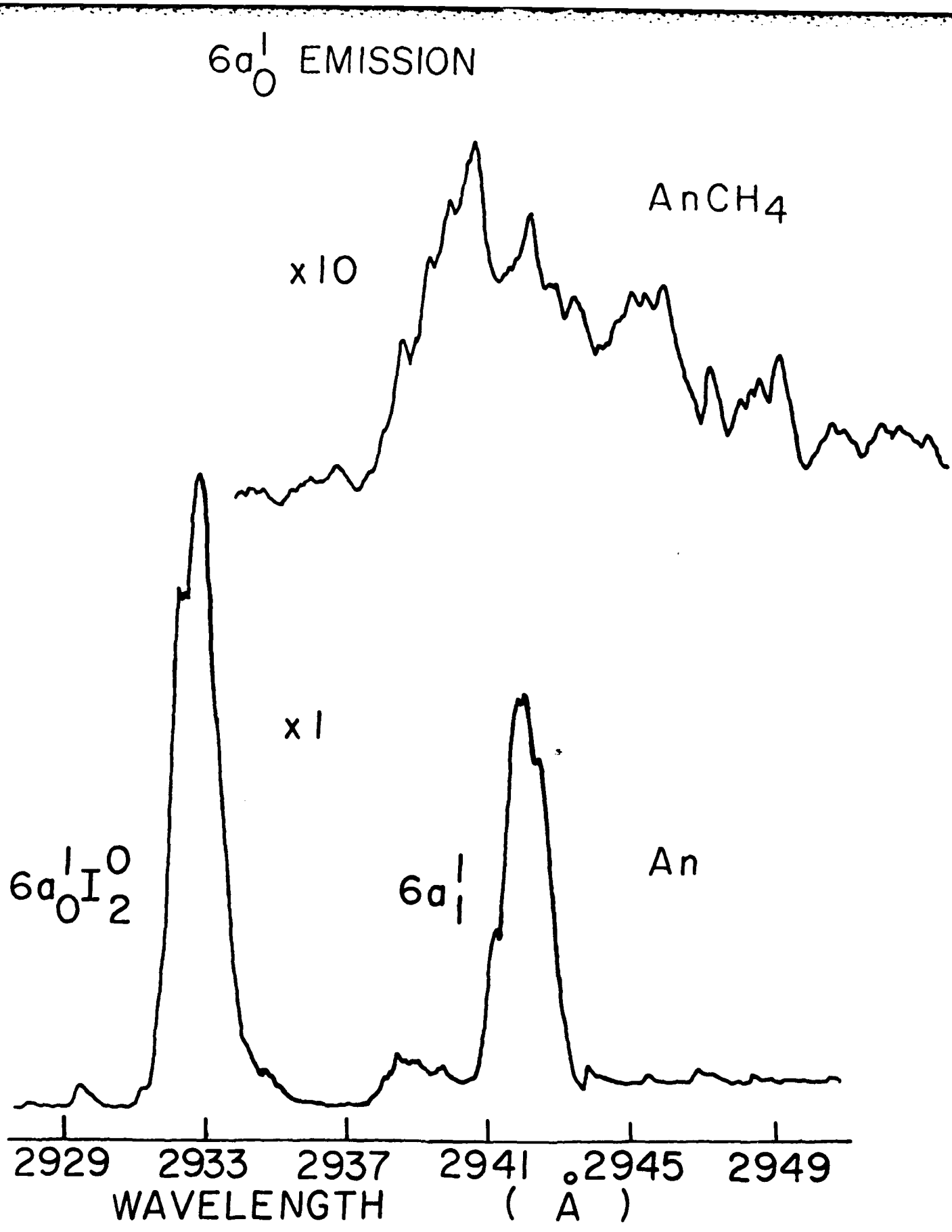
$6a_0^1$ EMISSION
AnCH4
x10
x1
$6a_0^1 I_2^0$
$6a_1^1$
An
2929
2933
2937
2941
2945
2949
WAVELENGTH (Å)

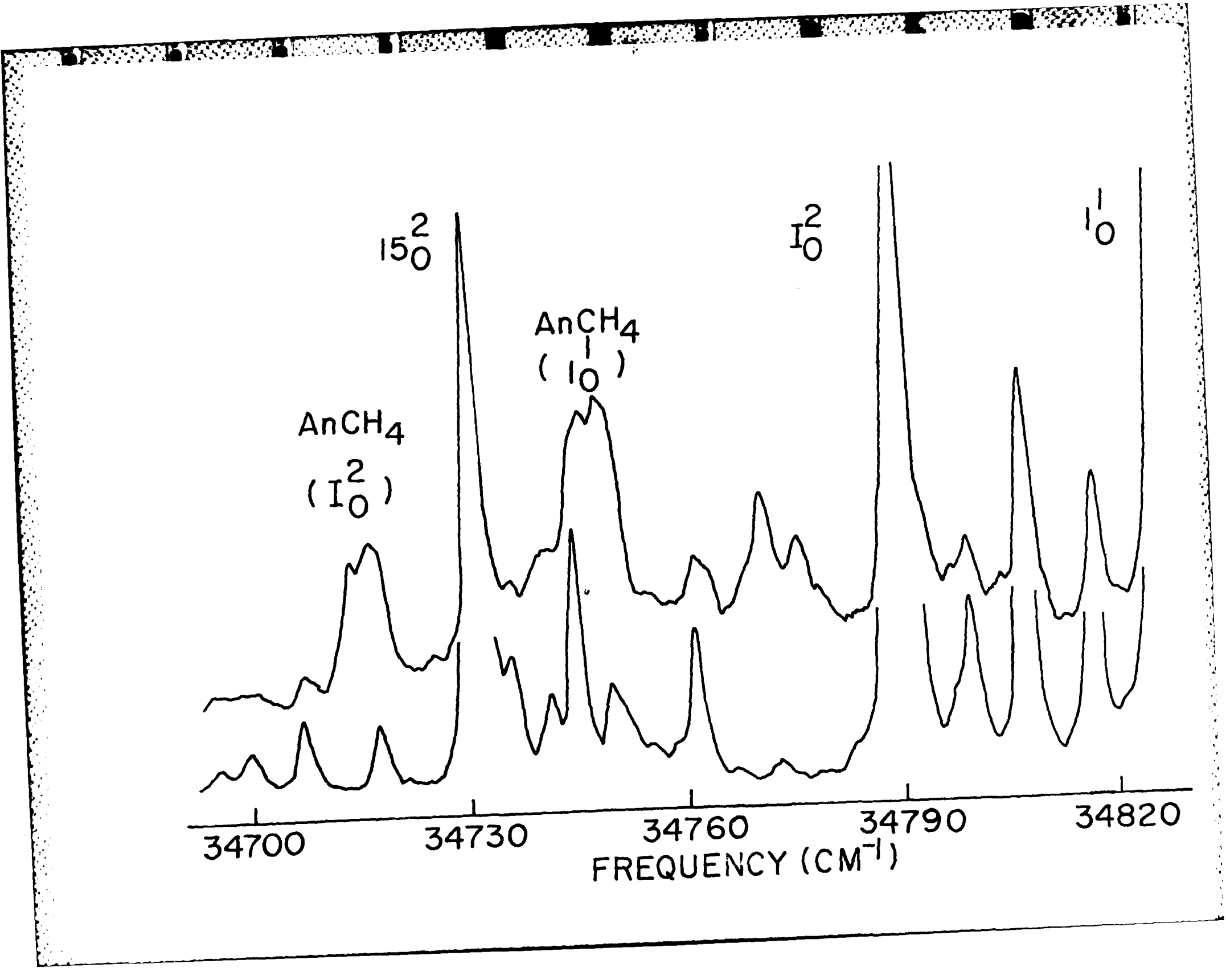
15_0^2
I_0^2
1_0^1
$AnCH_4$
(I_0^2)
$AnCH_4$
(1_0^1)
34700
34730
34760
34790
34820
FREQUENCY (CM^{-1})

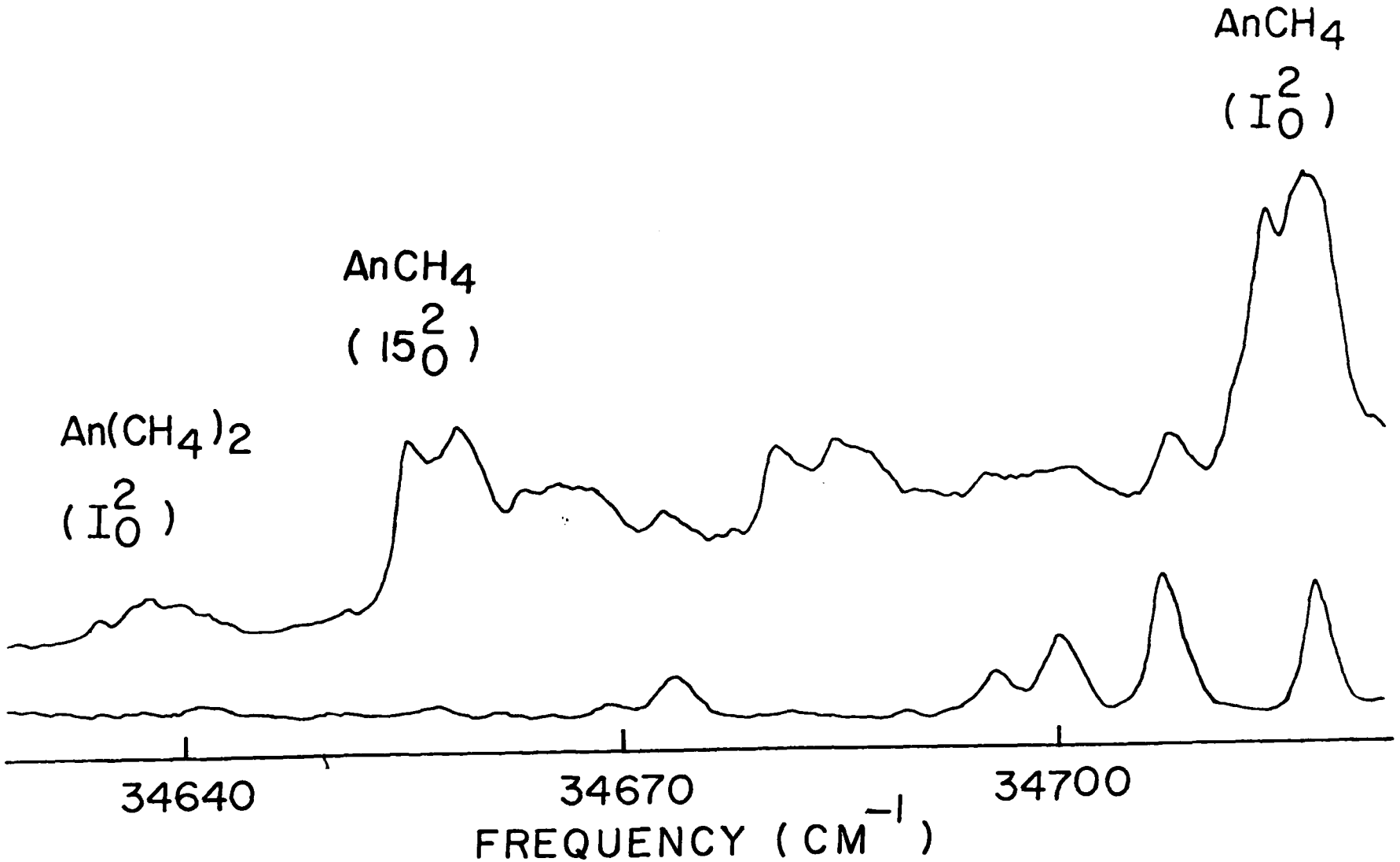
AnCH4
(I0 2)
AnCH4
(15 0 2)
An(CH4)2
(I0 2)
34640
34670
34700
FREQUENCY (CM-1)

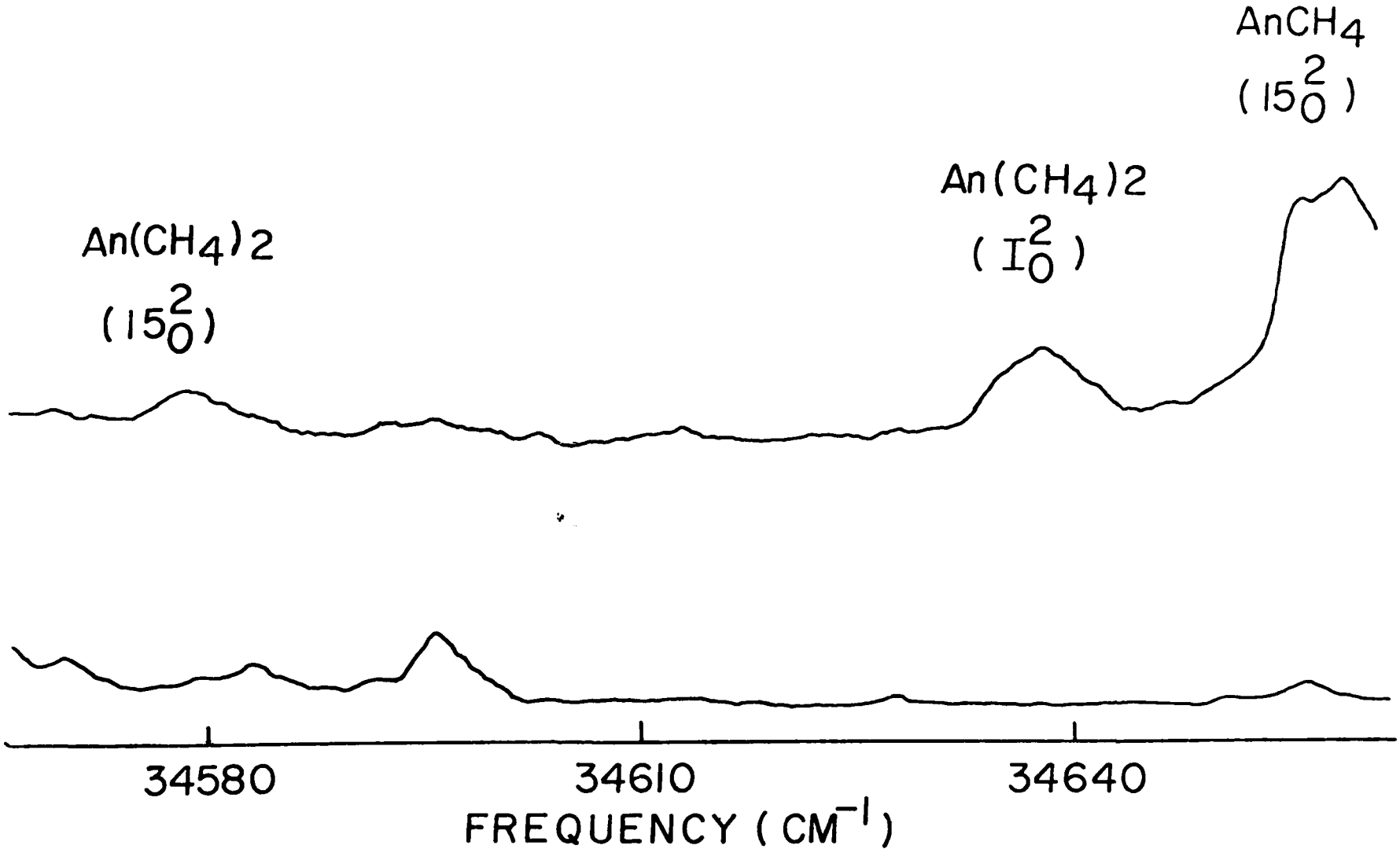
AnCH4
(15 0 2)
An(CH4)2
(I 0 2)
An(CH4)2
(15 0 2)
34580
34610
34640
FREQUENCY (CM-1)

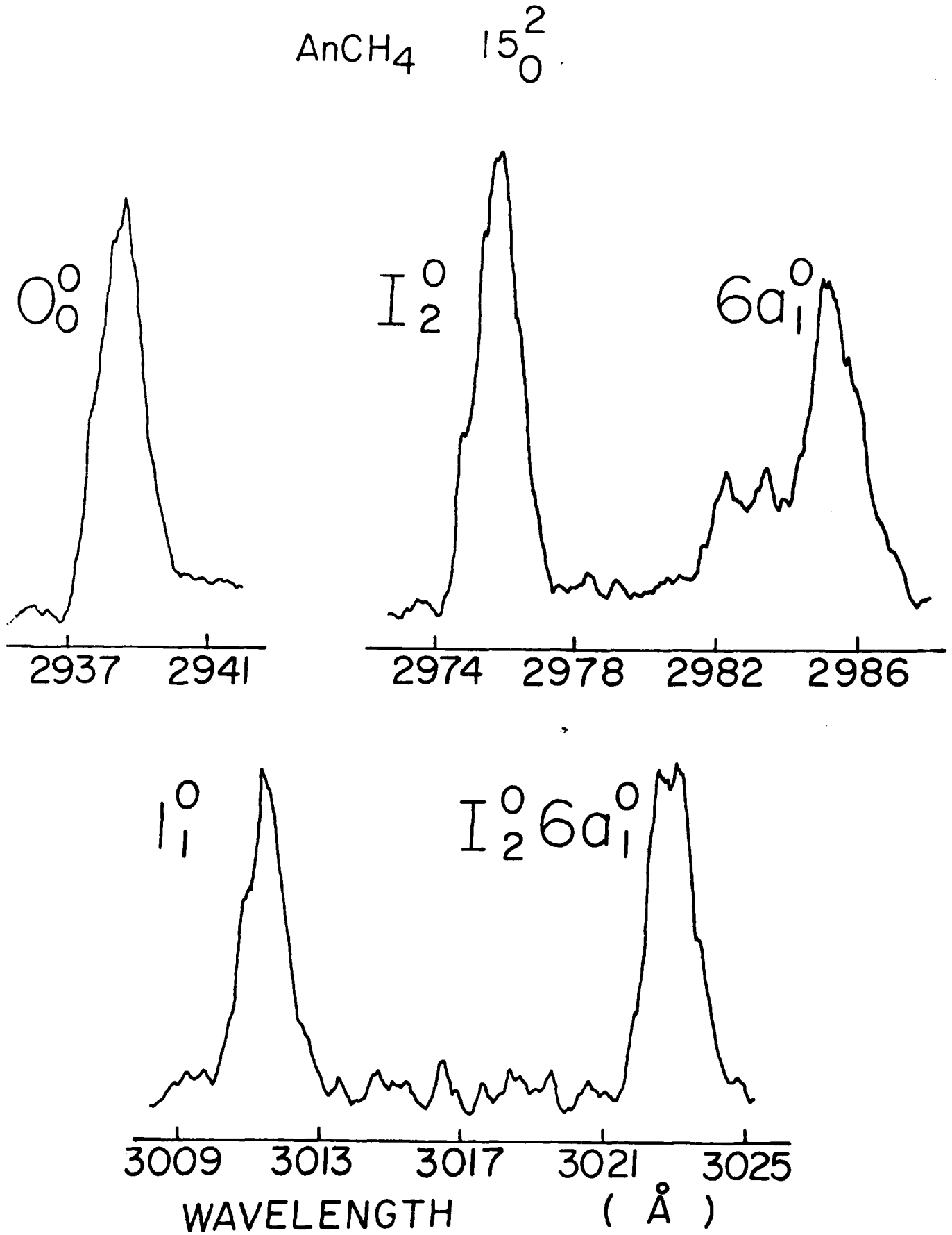
AnCH4 15 2 0
0 0 0
I 0 2
6a 0 1
1 0 1
I 0 2 6a 0 1
2937
2941
2974
2978
2982
2986
3009
3013
3017
3021
3025
WAVELENGTH (Å)

TECHNICAL REPORT DISTRIBUTION LIST, GEN

	No. Copies
Office of Naval Research Attn: Code 472 800 North Quincy Street Arlington, Virginia 22217	2
ONR Western Regional Office Attn: Dr. R. J. Marcus 1030 East Green Street Pasadena, California 91106	1
ONR Eastern Regional Office Attn: Dr. L. H. Peebles Building 114, Section D 666 Summer Street Boston, Massachusetts 02210	1
Director, Naval Research Laboratory Attn: Code 6100 Washington, D.C. 20390	1
The Assistant Secretary of the Navy (RE&S) Department of the Navy Room 4E736, Pentagon Washington, D.C. 20350	1
Commander, Naval Air Systems Command Attn: Code 310C (H. Rosenwasser) Department of the Navy Washington, D.C. 20360	1
Defense Technical Information Center Building 5, Cameron Station Alexandria, Virginia 22314	12
Dr. Fred Saalfeld Chemistry Division, Code 6100 Naval Research Laboratory Washington, D.C. 20375	1
U.S. Army Research Office Attn: CRD-AA-IP P.O. Box 1211 Research Triangle Park, N.C. 27709	1
Naval Ocean Systems Center Attn: Mr. Joe McCartney San Diego, California 92152	1
Naval Weapons Center Attn: Dr. A. B. Amster, Chemistry Division China Lake, California 93555	1
Naval Civil Engineering Laboratory Attn: Dr. R. W. Drisko Port Hueneme, California 93401	1
Department of Physics & Chemistry Naval Postgraduate School Monterey, California 93940	1
Scientific Advisor Commandant of the Marine Corps (Code RD-1) Washington, D.C. 20380	1
Naval Ship Research and Development Center Attn: Dr. G. Bosmajian, Applied Chemistry Division Annapolis, Maryland 21401	1
Naval Ocean Systems Center Attn: Dr. S. Yamamoto, Marine Sciences Division San Diego, California 91232	1
Mr. John Boyle Materials Branch Naval Ship Engineering Center Philadelphia, Pennsylvania 19112	1

TECHNICAL REPORT DISTRIBUTION LIST, GEN

	No. Copies
Mr. James Kelley DTNSRDC Code 2803 Annapolis, Maryland 21402	1
Mr. A. M. Anzalone Administrative Librarian PLASTEC/ARRADCOM Bldg 3401 Dover, New Jersey 07801	1

TECHNICAL REPORT DISTRIBUTION LIST, 051A

	No. Copies
Dr. M. A. El-Sayed Department of Chemistry University of California, Los Angeles Los Angeles, California 90024	1
Dr. C. A. Heller Naval Weapons Center Code 6059 China Lake, California 93555	1
Dr. J. R. MacDonald Chemistry Division Naval Research Laboratory Code 6110 Washington, D.C. 20375	1
Dr. G. B. Schuster Chemistry Department University of Illinois Urbana, Illinois 61801	1
Dr. A. Adamson Department of Chemistry University of Southern California Los Angeles, California 90007	1
Dr. M. S. Wrighton Department of Chemistry Massachusetts Institute of Technology Cambridge, Massachusetts 02139	1
Dr. M. Rauhut Chemical Research Division American Cyanamid Company Bound Brook, New Jersey 08805	1
Dr. J. I. Zink Department of Chemistry University of California, Los Angeles Los Angeles, California 90024	1
Dr. D. Haarer IBM San Jose Research Center 5600 Cottle Road San Jose, California 95143	1
Dr. John Cooper Code 6130 Naval Research Laboratory Washington, D.C. 20375	1
Dr. William M. Jackson Department of Chemistry Howard University Washington, DC 20059	1
Dr. George E. Walraffen Department of Chemistry Howard University Washington, DC 20059	1

END

FILMED

10-83

DTIC